




Topologically associating domains and chromatin loops depend on cohesin and are regulated by CTCF, WAPL, and PDS5 proteins

Gordana Wutz^{1,†}, Csilla Várnai^{2,†} , Kota Nagasaka^{1,†}, David A Cisneros^{1,†,‡}, Roman R Stocsits¹, Wen Tang¹, Stefan Schoenfelder², Gregor Jessberger¹, Matthias Muhar¹, M Julius Hossain³ , Nike Walther³, Birgit Koch³, Moritz Kueblbeck³, Jan Ellenberg³, Johannes Zuber¹, Peter Fraser^{2,4} & Jan-Michael Peters^{1,*} 

Abstract

Mammalian genomes are spatially organized into compartments, topologically associating domains (TADs), and loops to facilitate gene regulation and other chromosomal functions. How compartments, TADs, and loops are generated is unknown. It has been proposed that cohesin forms TADs and loops by extruding chromatin loops until it encounters CTCF, but direct evidence for this hypothesis is missing. Here, we show that cohesin suppresses compartments but is required for TADs and loops, that CTCF defines their boundaries, and that the cohesin unloading factor WAPL and its PDS5 binding partners control the length of loops. In the absence of WAPL and PDS5 proteins, cohesin forms extended loops, presumably by passing CTCF sites, accumulates in axial chromosomal positions (vermicelli), and condenses chromosomes. Unexpectedly, PDS5 proteins are also required for boundary function. These results show that cohesin has an essential genome-wide function in mediating long-range chromatin interactions and support the hypothesis that cohesin creates these by loop extrusion, until it is delayed by CTCF in a manner dependent on PDS5 proteins, or until it is released from DNA by WAPL.

Keywords chromatin condensation; chromatin structure; genome organization; loop extrusion; vermicelli

Subject Categories Chromatin, Epigenetics, Genomics & Functional Genomics; DNA Replication, Repair & Recombination

DOI 10.15252/embj.201798004 | Received 14 August 2017 | Revised 7 November 2017 | Accepted 7 November 2017 | Published online 7 December 2017

The EMBO Journal (2017) 36: 3573–3599

See also: **J Gassler et al** (December 2017) and **JHI Haarhuis & BD Rowland** (December 2017)

Introduction

Duplicated DNA molecules become physically connected with each other during DNA replication. This sister chromatid cohesion is essential for bi-orientation of chromosomes on the mitotic or meiotic spindle and thus enables their symmetrical segregation during cell division (Dewar *et al*, 2004). Cohesion is mediated by cohesin complexes (Guacci *et al*, 1997; Michaelis *et al*, 1997; Losada *et al*, 1998) which are thought to perform this function by entrapping both sister DNA molecules inside a ring structure that is formed by the cohesin subunits SMC1, SMC3, and SCC1 (also known as RAD21 and Mcd1) (Haering *et al*, 2008).

Cohesin is present at centromeres and on chromosome arms (reviewed in Peters *et al*, 2008). At centromeres, cohesin resists the pulling force of spindle microtubules, a function that is required both for stabilization of microtubule–kinetochore attachments and for chromosome bi-orientation. On chromosome arms, however, the precise location of cohesin would not be expected to matter if cohesin's only function was to mediate cohesion. But contrary to this expectation, cohesin is enriched at thousands of well-defined loci on chromosome arms. In mammalian genomes, ~90% of these are defined by binding sites for CCCTC binding factor (CTCF) (Parelho *et al*, 2008; Wendt *et al*, 2008). CTCF is a zinc-finger protein that has been implicated in various aspects of gene regulation, such as insulating gene promoters from distant enhancers (reviewed in Wendt & Peters, 2009). Early work revealed that this enhancer-blocking activity is required for imprinted gene expression at the *H19-IGF2 locus* (Bell & Felsenfeld, 2000; Hark *et al*, 2000) and indicated that CTCF mediates this function by creating allele-specific chromatin loops (Kurukuti *et al*, 2006; Splinter *et al*, 2006). Remarkably, cohesin is also required for CTCF's enhancer blocking activity at the *H19-IGF2 locus* (Wendt *et al*, 2008) and the chicken

1 Research Institute of Molecular Pathology (IMP), Vienna Biocenter (VBC), Vienna, Austria

2 Nuclear Dynamics Programme, The Babraham Institute, Babraham Research Campus, Cambridge, UK

3 Cell Biology and Biophysics Unit, European Molecular Biology Laboratory, Heidelberg, Germany

4 Department of Biological Science, Florida State University, Tallahassee, FL, USA

*Corresponding author. Tel: +43 1797303000; E-mail: peters@imp.ac.at

†These authors contributed equally to this work

‡Present address: The Laboratory for Molecular Infection Medicine Sweden (MIMS) and Department of Molecular Biology, Umeå University, Umeå, Sweden

β -globin locus (Parelho *et al.*, 2008), as well as for regulation of other genes reviewed in (Wendt & Peters, 2009; Dorsett & Merkenschlager, 2013). Importantly, these requirements have been identified in G1-phase of the cell cycle and in post-mitotic cells, in which cohesin is also present, indicating that they are not an indirect effect of cohesin's role in sister chromatid cohesion but reflect an independent function of cohesin (Pauli *et al.*, 2008; Wendt *et al.*, 2008).

Because cohesin is required for CTCF-dependent gene regulation events that are thought to be mediated by chromatin looping, and because cohesin is well known to be able to physically connect distinct DNA elements to generate cohesion, it has been proposed that cohesin can also generate or stabilize chromatin loops (Wendt *et al.*, 2008; Wendt & Peters, 2009). According to this hypothesis, cohesin would not only be able to connect two sister DNA molecules in *trans* to generate cohesion, but would also be able to connect regions on the same chromatid in *cis*. This hypothesis has been supported by chromatin conformation capture (3C) experiments which indicated that long-range chromosomal *cis*-interactions at the apolipoprotein gene cluster, the γ -interferon, and *H19-IGF2 loci* (Hadjur *et al.*, 2009; Mishiro *et al.*, 2009; Nativio *et al.*, 2009) as well as enhancer–promoter interactions (Kagey *et al.*, 2010) are dependent on cohesin.

Evidence for a role of cohesin in chromatin structure has also come from experiments in which the cohesin-associated protein WAPL was depleted. WAPL can release cohesin from DNA (Gandhi *et al.*, 2006; Kueng *et al.*, 2006; Tedeschi *et al.*, 2013), presumably by opening the cohesin ring (Kueng *et al.*, 2006; Chan *et al.*, 2012; Huis in 't Veld *et al.*, 2014), and WAPL depletion, therefore, increases residence time and amounts of cohesin on DNA (Kueng *et al.*, 2006; Tedeschi *et al.*, 2013). Remarkably, this causes mild but global compaction of chromatin (Tedeschi *et al.*, 2013), indicating that the effects of cohesin on chromatin architecture are widespread and not confined to a few *loci*.

Unexpectedly, WAPL depletion also causes a dramatic intranuclear re-localization of cohesin. Cohesin is normally detectable in most regions of interphase chromatin (Losada *et al.*, 1998; Sumara *et al.*, 2000), but after WAPL depletion, it accumulates in axial structures called “vermicelli” which are thought to extend along the entire length of interphase chromosome territories (Tedeschi *et al.*, 2013). Vermicelli are reminiscent of axial elements in mitotic and meiotic chromosomes. These structures contain condensin and meiosis-specific cohesin complexes, respectively, and are thought to form the base of chromatin loops, into which chromatin fibers are organized during chromosome condensation (Earnshaw & Laemmli, 1983; Saitoh *et al.*, 1994; Klein *et al.*, 1999; Blat *et al.*, 2002; Ono *et al.*, 2003; Yeong *et al.*, 2003). It has, therefore, been proposed that vermicelli represent cohesin complexes that are located at the base of loops in interphase chromatin, and that vermicelli become detectable only after WAPL depletion because increased residence time and amounts of cohesin lead to the formation or stabilization of more chromatin loops than normally (Tedeschi *et al.*, 2013).

Interestingly, both chromatin compaction and accumulation of cohesin axial structures are predicted to occur in WAPL-depleted cells if one assumes that cohesin forms chromatin loops *via* a hypothetical loop extrusion process (Fudenberg *et al.*, 2016). According to this idea, two distal chromosomal elements would be brought into direct proximity by a loop extrusion factor such as

cohesin which would processively extrude a chromatin loop (Riggs, 1990; Nasmyth, 2001; Alipour & Marko, 2012; Gruber, 2014; Sanborn *et al.*, 2015; Fudenberg *et al.*, 2016). Since WAPL depletion increases cohesin's residence time on DNA, cohesin would extrude longer loops and cohesin complexes would come into closer proximity than normally, resulting in chromatin compaction and vermicelli formation, respectively. *In silico* modeling of DNA folding has confirmed these predictions (Fudenberg *et al.*, 2016).

Importantly, the loop extrusion hypothesis can also explain the “CTCF convergence rule” (Rao *et al.*, 2014; Vietri Rudan *et al.*, 2015; de Wit *et al.*, 2015). This describes the unexpected phenomenon that CTCF binding sites that form the base of chromatin loops are typically oriented toward each other. The DNA sequences with which CTCF can associate are not palindromic (symmetrical), that is, could be positioned relative toward each other in convergent, tandem, or divergent orientations. If CTCF sites formed loops by random association, they would be expected to occur in convergent, tandem, and divergent orientations with frequencies of 25, 50, and 25%, respectively. However, high-resolution genome-wide chromatin conformation capture experiments coupled with DNA sequencing (“Hi-C”) (Lieberman-Aiden *et al.*, 2009) have revealed that most chromatin loops contain convergent CTCF sites (Rao *et al.*, 2014; Vietri Rudan *et al.*, 2015; de Wit *et al.*, 2015). This would be expected if these sites were brought into proximity by loop extrusion, but cannot be explained if these sites found each other by random diffusion (Sanborn *et al.*, 2015; Fudenberg *et al.*, 2016). Based on these observations and considerations, it has been proposed that CTCF sites function as directional boundary elements during loop extrusion (Sanborn *et al.*, 2015; Fudenberg *et al.*, 2016). However, for cohesin to be able to form extended loops in WAPL-depleted cells, as proposed by Fudenberg *et al.* (2016), these boundaries would have to be permeable to some extent.

The notion that CTCF sites can function as boundary elements for loop extrusion is consistent with the observation that cohesin and CTCF co-localize (Parelho *et al.*, 2008; Wendt *et al.*, 2008), and that many of these sites either form the base of chromatin loops (Rao *et al.*, 2014), or are enriched at the boundaries of more complex chromatin structures, called topologically associating domains (TADs) (Dixon *et al.*, 2012; Nora *et al.*, 2012). These are covering chromosomal regions, typically up to 1 Mb in length, in which long-range chromosomal *cis*-interactions occur with increased frequencies. At the level of individual cells, TADs may represent loops that are in the process of being extruded to various degrees. In support of this idea, it has been proposed based on single-nucleus Hi-C experiments that TADs emerge from averaging interactions in large cell populations (Flyamer *et al.*, 2017). Importantly, genome-editing experiments in which CTCF sites were deleted or inverted indicate that these are indeed required for the formation of TAD boundaries (Nora *et al.*, 2012; Narendra *et al.*, 2015; Sanborn *et al.*, 2015; de Wit *et al.*, 2015).

The hypothesis that cohesin contributes to the formation of TADs and loops by mediating loop extrusion is also consistent with the observation that cohesin can move along DNA, both *in vitro* (Davidson *et al.*, 2016; Kanke *et al.*, 2016; Stigler *et al.*, 2016) and *in vivo* (Lengronne & Pasero, 2014; Busslinger *et al.*, 2017) and is constrained during these movements by CTCF (Davidson *et al.*, 2016; Busslinger *et al.*, 2017). In contrast, cohesin and CTCF are not

thought to contribute to chromatin organization at levels above TADs and loops (i.e., covering larger genomic regions), at which Hi-C experiments have identified higher-order structures called A and B compartments (Lieberman-Aiden *et al*, 2009). Both of these exist in different sub-types (Rao *et al*, 2014; Nagano *et al*, 2017) and are thought to represent euchromatic and heterochromatic regions, respectively.

However, even though the above-mentioned observations indicate that cohesin and CTCF may have important roles in the formation of TADs and loops, previous Hi-C experiments found that inactivation of cohesin or CTCF had only modest effects on chromatin organization (Seitan *et al*, 2013; Sofueva *et al*, 2013; Zuin *et al*, 2014). It is, therefore, incompletely understood whether cohesin and CTCF have important roles in chromatin organization, and if so, whether these are mediated by loop extrusion.

We have, therefore, further analyzed the roles of cohesin and CTCF in chromatin organization by using microscopic imaging and Hi-C experiments. For this purpose, we have either inactivated cohesin or CTCF by conditional proteolysis (Nishimura *et al*, 2009), or stabilized cohesin on DNA by depleting WAPL and its binding partners PDS5A and PDS5B (Kueng *et al*, 2006). Our experiments indicate that cohesin is required for the formation and/or maintenance of TADs and loops but suppresses compartments, that WAPL and PDS5 proteins antagonize these functions, and that CTCF is required for the formation of “sharp” boundaries between TADs and the formation of loops by defined loop anchors. We also show that co-depletion of WAPL, PDS5A, and PDS5B enables cohesin to condense chromosomes to an extent that is normally only seen in early mitosis by creating long-range chromosomal *cis*-interactions that are reminiscent of the ones observed in mitotic chromosomes (Naumova *et al*, 2013; Nagano *et al*, 2017). These observations are consistent with the loop extrusion hypothesis. Unexpectedly, however, our results indicate that PDS5 proteins, which are thought to cooperate with WAPL in releasing cohesin from DNA (Rowland *et al*, 2009; Shintomi & Hirano, 2009; Ouyang *et al*, 2016), have a function in chromatin loop formation that is distinct from the role of WAPL and that may be required for CTCF’s ability to function as a boundary element for loop extrusion.

Cohesin, CTCF and WAPL, but not PDS5 proteins, have also been inactivated in other recent Hi-C studies which were deposited on *bioRxiv* (Kubo *et al*, 2017) or published in peer-reviewed journals during preparation or after submission of our manuscript (Gassler *et al*, 2017; Haarhuis *et al*, 2017; Rao *et al*, 2017; Schwarzer *et al*, 2017). We compare and contrast the results of these as well as the earlier studies (Seitan *et al*, 2013; Sofueva *et al*, 2013; Zuin *et al*, 2014) with ours in the Discussion.

Results

Acute cohesin inactivation by auxin-mediated degradation

To analyze cohesin’s role in chromatin structure, we modified all SCC1 alleles in HeLa cells by CRISPR-Cas9-mediated genome editing to encode proteins in which SCC1 is C-terminally fused to monomeric enhanced green fluorescent protein (mEGFP) and an

auxin-inducible degron (AID; Fig 1A). To enable auxin-dependent recognition of SCC1-mEGFP-AID by SCF ubiquitin ligases, we stably expressed the *Oryza sativa* F-box transport inhibitor response-1 auxin receptor protein (Tir1) in these cells. In immunoblotting experiments, only SCC1-mEGFP-AID but no untagged SCC1 could be detected, confirming that all SCC1 alleles had been modified (Fig 1B). These experiments also revealed that mEGFP-AID tagging reduced SCC1 levels (Fig 1B), consistent with the finding that C-terminal tagging compromises SCC1 function in mice (Tachibana-Konwalski *et al*, 2010). Cells expressing only SCC1-mEGFP-AID nevertheless proliferated at similar rates as wild-type cells, indicating that cohesin complexes containing this fusion protein can perform their essential cellular functions and are present in copy numbers sufficient for this.

Auxin addition reduced GFP fluorescence intensity to “background” levels in 20 min in cells expressing Tir1, but not in cells lacking Tir1 (Fig 1C and D). Immunoblotting experiments confirmed that loss of fluorescence intensity was caused by SCC1-mEGFP-AID degradation and showed that it resulted in concomitant release of the cohesin subunits SMC1 and SMC3 from chromatin, whereas CTCF and the cohesin loading complex NIPBL-MAU2 remained chromatin-associated (Figs 1E and EV1A).

Cohesin inactivation strengthens compartments but weakens TADs and loops

To analyze the effects of cohesin inactivation on chromatin structure, we synchronized SCC1-mEGFP-AID cells in G1-phase by double-thymidine arrest–release, treated them for 0, 15, or 180 min with auxin, and measured chromatin interactions genome-wide by Hi-C (Fig 1F–J). In a separate experiment, we analyzed the same cells after 0 and 120 min of auxin treatment (Fig EV2; all Hi-C libraries analyzed in this study and their properties are listed in Table EV1). All genome-wide interaction matrices were analyzed for the presence of five types of patterns which have been observed in Hi-C data from mammalian genomes: *cis-trans* interaction ratios, distance-dependent interaction frequencies at the genomic level, compartments, TADs, and point interactions (“loops”) at specific genomic positions (Lajoie *et al*, 2015). Importantly, none of these patterns differed significantly between Hi-C matrices obtained from cells collected at the 0 min time points of the two experiments, indicating that changes observed in auxin-treated cells were caused by cohesin degradation and not inter-experimental variation.

Cis-trans interaction ratios were high in all cases, with inter-chromosomal interactions only representing 5–15%, indicating that all Hi-C libraries were of high quality. However, *trans* interactions were consistently higher in cohesin-depleted cells (Table EV1). Contact frequencies were affected differently by cohesin inactivation, depending on genomic distances between contacting loci. Cohesin depletion gradually decreased contact frequencies at 100 kb–1 Mb distances, while the frequency of long-range (> 10 Mb) interactions increased (Fig 1F). Cohesin inactivation might therefore enable more contacts with distant parts of chromosomes and even neighboring chromosomes, possibly because chromatin structure becomes more flexible under these conditions. For reasons explained in the next paragraph, we do not believe that these changes are caused by technical artifacts, such as increased “noise” in the Hi-C libraries.

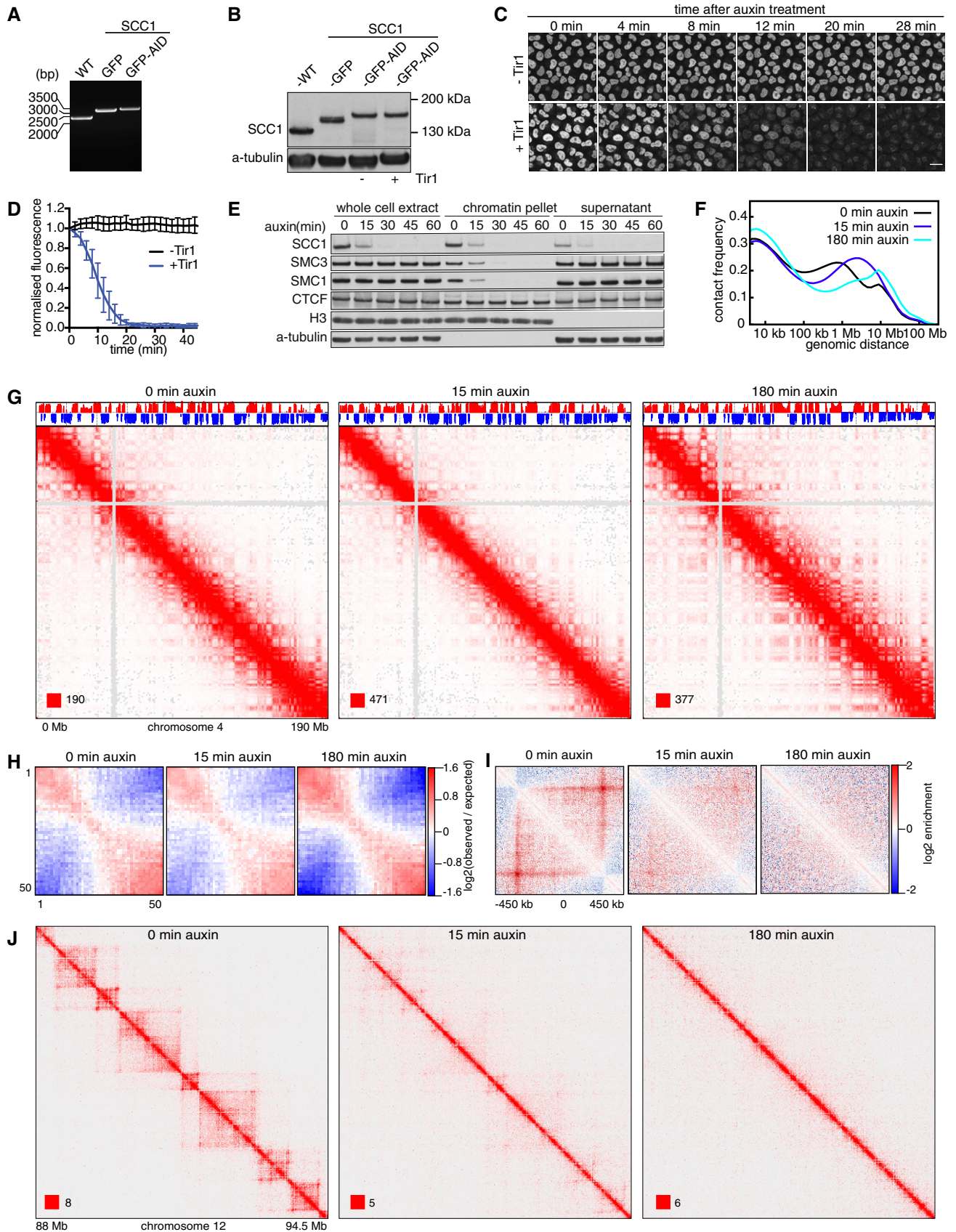


Figure 1.

Figure 1. Chromatin organization changes upon auxin-induced SCC1 degradation.

- A Genotype analysis of parental HeLa cells (WT), homozygous SCC1-mEGFP cells (GFP), and homozygous SCC1-mEGFP-AID cells (GFP-AID). Genomic PCR products were generated with the primers that are designed external to the homology arm which was used for inserting mEGFP or mEGFP-AID encoding sequences downstream of the SCC1 gene. This resulted in fusion proteins with mEGFP or mEGFP-AID tags C-terminal to the SCC1 gene.
- B Immunoblotting analysis of whole-cell extracts from parental HeLa WT cells, SCC1-mEGFP cells, SCC1-mEGFP-AID (–) cells (i.e., not expressing Tir1), and SCC1-mEGFP-AID cells expressing Tir1 (+). α -Tubulin: loading control.
- C Time course live-cell imaging of SCC1-mEGFP-AID cells after auxin treatment. SCC1-mEGFP-AID cells with (+) or without (–) Tir1 were imaged after addition of auxin. Scale bar indicates 20 μ m.
- D Quantification of nuclear GFP signal over time after auxin addition to SCC1-mEGFP-AID cells with (+) or without (–) Tir1. Normalized nuclear GFP signals are plotted over time after addition of Auxin into –Tir1 and +Tir1 cells (mean \pm SD). $n = 9$ cells per condition.
- E Chromatin fractionation and immunoblot analysis of auxin-treated SCC1-mEGFP-AID cells expressing Tir1. At the indicated time points after auxin addition, whole-cell extracts, the chromatin pellet fraction, and the supernatant fraction were analyzed by immunoblotting, using antibodies against the proteins indicated on the left.
- F Intra-chromosomal contact frequency distribution as a function of genomic distance, at 0 (black), 15 (blue), and 180 min (cyan) after auxin addition to SCC1-mEGFP-AID cells expressing Tir1.
- G Coverage-corrected Hi-C contact matrices of chromosome 4, at 0 (left), 15 (center), and 180 min (right) after auxin addition to SCC1-mEGFP-AID cells expressing Tir1. The corresponding compartment signal tracks at 250 kb bin resolution are shown above the matrices. The matrices were plotted using Juicebox.
- H Long-range (> 2 Mb) intra-chromosomal contact enrichment between bins with varying compartment signal strength from most B-like (1) to most A-like (50).
- I Average contact enrichment around loops after auxin addition to SCC1-mEGFP-AID cells expressing Tir1, for the 82 \times 600 kb long loops identified in G1 control HeLa cells. The matrices are centered (0) around the halfway point of the loop anchor coordinates.
- J For the same conditions as in (G–I), coverage-corrected Hi-C contact matrices in the 88–94.5 Mb region of chromosome 12, plotted using Juicebox.
- Source data are available online for this figure.

Cohesin degradation also induced major changes at the level of compartments, TADs, and loops. In cells treated for 120 or 180 min with auxin, A and B compartments could be detected more clearly than in control cells (Table EV1), as coverage-corrected maps of single chromosomes showed increased interaction frequencies further away from the diagonal of the Hi-C matrices, resulting in enhanced “plaid” or “checkerboard” patterns (Figs EV2A and 1G). Genome-wide aggregate analysis of 50 compartment categories ranging from strong B to strong A compartments genome-wide confirmed this, showing increasing contact enrichment between similar compartment categories and a decreasing contact enrichment between dissimilar (e.g., strong A and strong B) compartment bins in both long *cis* (> 2 Mb, Figs EV2C and 1H) and *trans* interactions. The strengthened compartmentalization suggests that the increase in long-range contact frequencies described above was not due to “noise” in the Hi-C libraries, since more long-range random contacts would result in less contact specificity and a weakening in compartmentalization strength.

Whereas compartments became more apparent in cohesin-depleted cells, TADs were greatly reduced (Figs EV2B and 1J). After auxin addition, there was a gradual decrease in TAD detectability based on directionality indices (Dixon *et al*, 2012), with the genome coverage of identified TADs decreasing from 56% in control cells to 52% and 44% after 15 and 180 min of auxin treatment, respectively. Aggregate TAD analysis confirmed this (Figs EV1B and EV2D). The insulation score calculated for TAD borders declined concomitant with the disappearance of TADs (Fig EV1C). It is important to note that the fact that TADs could still be called in 44% of the genome after SCC1 degradation is in part an effect of the TAD calling method we used in which directionality indices are standardized. This approach increases the detectability of boundaries for samples with weakened domain structures, because weak raw directionality index signals are comparatively magnified by this standardization (Nagano *et al*, 2015).

Individual loops also disappeared gradually following cohesin degradation until they were barely detectable after 180 min; in this

experiment, “juicer-tool” (Rao *et al*, 2014) identified 5,740 loops in control cells, but only 204 (3.6%) after 180 min of auxin treatment (Fig EV1D; aggregate analyses of loops 600 kb in length are shown in Figs 1I and EV2E and of 0.75–6 Mb loops in Figs EV1E and EV2F). In this context, it is important to note that the number of loops that can be called depends on the number of replicate Hi-C libraries sequenced, with more replicate numbers yielding higher signal-to-noise ratios and thus higher loop numbers. In each given experiment of this study, we, therefore, compared data from identical numbers of replicates. However, because different replicate numbers were sequenced in different experiments, the absolute number of loops identified varies between experiments (see below).

These results indicate that local genome organization into TADs and loops depends critically on cohesin and changes rapidly after its inactivation, whereas cohesin suppresses the formation of A and B compartments or their detectability by Hi-C. Interestingly, after 15 min auxin treatment, most loops and TADs became undetectable to the eye, whereas enhanced compartmentalization was only observed after 180 min of auxin treatment. Loops and TADs are therefore particularly sensitive to cohesin inactivation, whereas changes in compartments occur on a longer time scale.

For comparison, we also analyzed HeLa cells in which SCC1 was not tagged (Appendix Fig S1A–G). Unexpectedly, contact frequencies at 20 kb–1 Mb distances were higher in these than in SCC1-mEGFP-AID cells, while the frequency of long-range (> 2 Mb) interactions was lower (Appendix Fig S1A). The boundary insulation score and the number of loops that could be called were also higher in unmodified than in SCC1-mEGFP-AID expressing cells, as if chromatin was more highly organized in the former than the latter cells (Appendix Fig S1B and C). We suspect that these differences are caused by the reduced expression levels of SCC1-mEGFP-AID (see Fig 1B) and/or by functional defects caused by SCC1 tagging, such as reduced rate or processivity of loop extrusion.

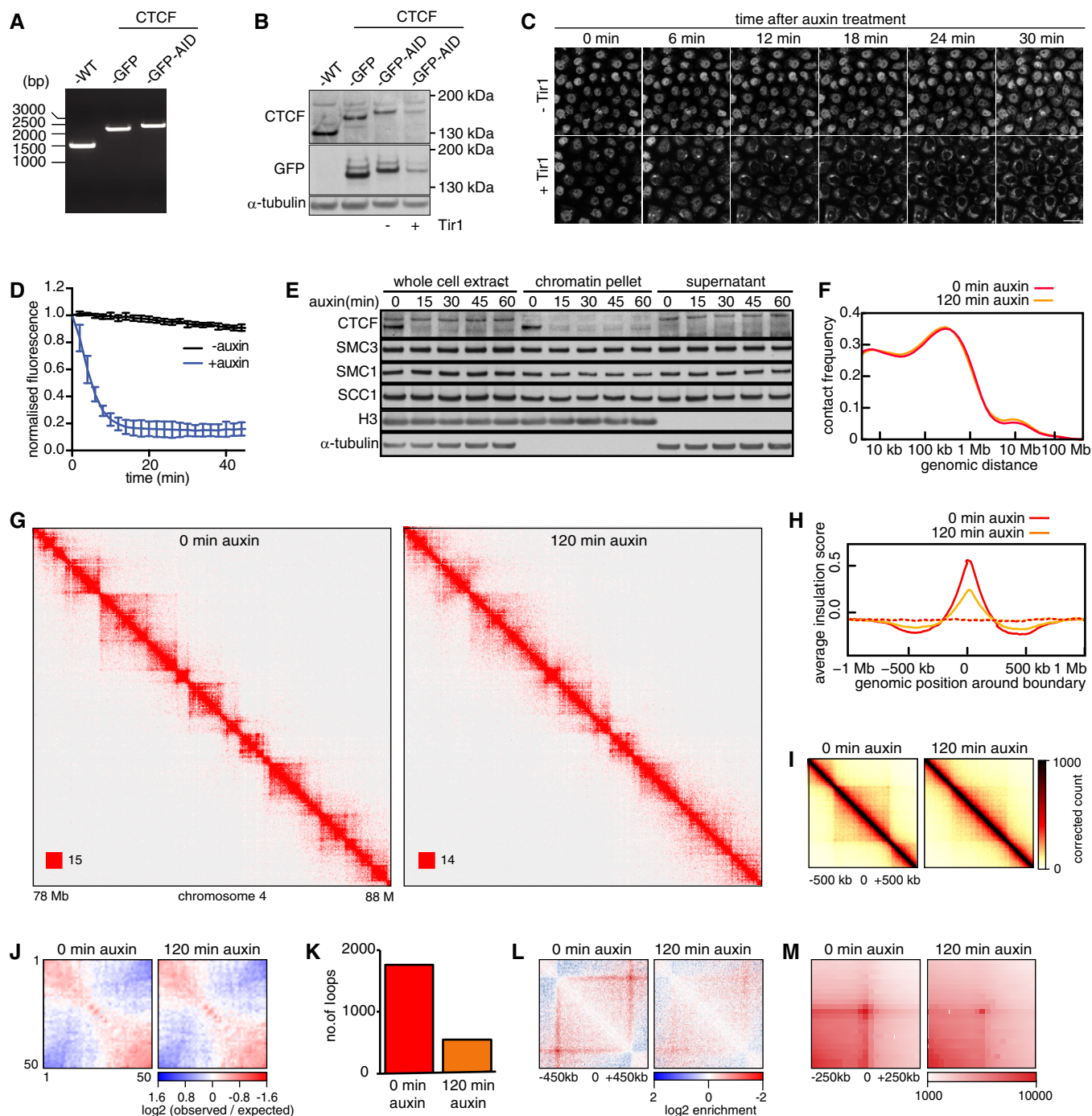


Figure 2.

Acute CTCF inactivation by auxin-mediated degradation

To analyze CTCF’s role in chromatin structure, we generated HeLa cells in which all CTCF alleles were modified to encode CTCF-mEGFP-AID (Fig 2A). Immunoblotting revealed that Tir1 expression reduced CTCF-mEGFP-AID levels even in the absence of auxin (Fig 2B), implying that Tir1 targets some CTCF-mEGFP-AID for degradation on its own. However, these cells proliferated at similar rates as wild-type cells, indicating that the functionality and copy

number of CTCF-mEGFP-AID are sufficient for cell viability and proliferation.

Auxin addition reduced the fluorescence intensity of CTCF-mEGFP-AID to “background” levels in 15 min (Fig 2C and D). GFP signals were low in these cells, consistent with the low CTCF-mEGFP-AID levels observed by immunoblotting. CTCF-mEGFP-AID could thus only be detected under imaging conditions which also revealed cytoplasmic fluorescence. However, this cytoplasmic signal did not disappear following auxin treatment, indicating that it was

Figure 2. Chromatin organization changes upon auxin-induced CTCF degradation.

- A Genotype analysis of parental HeLa cells (WT), homozygous CTCF-mEGFP cells (GFP), and homozygous CTCF-mEGFP-AID cells (GFP-AID). Genomic PCR products were generated with the primers that are designed external to the homology arm which was used for inserting mEGFP or mEGFP-AID encoding sequences downstream of the CTCF gene. This resulted in fusion proteins with mEGFP or mEGFP-AID tags C-terminal to the CTCF gene.
- B Immunoblotting analysis of whole-cell extracts from parental HeLa WT cells, CTCF-mEGFP cells, CTCF-mEGFP-AID (–) cells (i.e., not expressing Tir1), and CTCF-mEGFP-AID cells expressing Tir1 (+). α -Tubulin: loading control.
- C Time course live-cell imaging of CTCF-mEGFP-AID cells after auxin treatment. CTCF-mEGFP-AID cells with (+) or without (–) Tir1 were imaged after addition of auxin. Scale bar indicates 20 μ m.
- D Quantification of nuclear GFP signal over time after auxin addition to CTCF-mEGFP-AID cells with (+) or without (–) Tir1. Normalized nuclear GFP signals are plotted over time after addition of Auxin into –Tir1 and +Tir1 cells (mean \pm SD). $n = 9$ cells per condition.
- E Chromatin fractionation and immunoblot analysis of auxin-treated CTCF-mEGFP-AID cells expressing Tir1. At the indicated time points after auxin addition, whole-cell extracts, the chromatin pellet fraction, and the supernatant fraction were analyzed by immunoblotting, using antibodies against the proteins indicated on the left.
- F Intra-chromosomal contact frequency distribution as a function of genomic distance, 0 (red) and 120 min (yellow) after auxin addition to CTCF-mEGFP-AID cells expressing Tir1.
- G Coverage-corrected Hi-C contact matrices of chromosome 4 (78–88 Mb), 0 (left), and 120 min (right) after auxin addition to CTCF-mEGFP-AID cells expressing Tir1. The matrices were plotted using Juicebox.
- H Average insulation score around TAD boundaries identified in control-depleted G1 cells, for samples at 0 (red) and 120 min (yellow) after auxin addition to CTCF-mEGFP-AID cells expressing Tir1. Dashed lines show the average insulation score around the +1 Mb shifted boundaries as control.
- I Aggregate TAD analysis for CTCF-mEGFP-AID cells expressing Tir1, 0 (left) and 120 min (right) after auxin addition. Average coverage-corrected Hi-C contact matrices are shown centered around the 166 \times 500–550 kb long TADs identified in the control-depleted HeLa cells.
- J Long-range (> 2 Mb) intra-chromosomal contact enrichment between bins with varying compartment signal strength from most B-like (1) to most A-like (50), in the same conditions as (F).
- K Number of loops identified by HiCCUPS, in the same conditions as (F–H).
- L Average contact enrichment around loops after auxin addition to CTCF-mEGFP-AID cells expressing Tir1, for the 82 \times 600 kb long loops identified by HiCCUPS in control-depleted G1 cells. The matrices are centered (0) around the halfway point of the loop anchor coordinates.
- M Total contact counts around loops after auxin addition, for all 750 kb–6 Mb long loops identified by HiCCUPS in G1 control. The vertical and horizontal axes of the matrices were centered around the upstream and the downstream loop anchors, respectively.

Source data are available online for this figure.

caused by auto-fluorescent molecules other than mEGFP. Immunoblotting confirmed that auxin induces rapid degradation of most CTCF-mEGFP-AID (Fig 2E).

CTCF inactivation reduces the insulation between TADs

To analyze the effects of CTCF inactivation on chromatin structure, we synchronized CTCF-mEGFP-AID cells in G1-phase, treated them for 0 and 120 min with auxin, and measured chromatin interactions genome-wide by Hi-C (Fig 2F–M). CTCF degradation did not change contact frequencies at any contact distances (Fig 2F), including inter-chromosomal contacts (Table EV1). The long-range *cis*- and *trans*-chromosomal compartmentalization strength was also unaffected (Fig 2J and Table EV1). However, CTCF inactivation had a pronounced effect on TAD boundaries, which appeared fuzzier and less well defined than in control cells (Fig 2G and I). This was reflected by a strong decrease in the TAD insulation score (Fig 2H) and resulted in a reduction in the genome coverage of TADs as identified by directionality indices (from 58.4 to 50.8%). Likewise, most loops disappeared in cells depleted of CTCF; “juicer-tool” identified 1,763 loops before auxin addition, but only 546 loops 120 min after auxin addition (Fig 2K). This number of loops (1,763) is much smaller than the number identified in unmodified HeLa cells (5,740; Appendix Fig S1C), in which also the TAD insulation score is higher (Appendix Fig S1B). As for SCC1-mEGFP-AID cells, we, therefore, suspect that CTCF-mEGFP-AID cells are hypomorphic with respect to CTCF function, either because of their reduced CTCF levels or because of functional interference from the mEGFP-AID tag.

Together, these results indicate that CTCF has a distance-independent role in chromatin organization, is not essential for

compartmentalization, but is required for the formation and/or maintenance of TAD borders and the detectability of loops. These observations imply that CTCF, unlike cohesin, is not required for long-range chromatin interactions *per se*, but has an important role in defining their precise position, consistent with the proposed role of CTCF as a boundary for loop extrusion (Sanborn *et al*, 2015; Fudenberg *et al*, 2016).

PDS5 proteins cooperate with WAPL in controlling cohesin localization and chromatin structure

Our results so far indicated that cohesin is required for the formation and/or maintenance of TADs and loops, but suppresses compartmentalization, whereas CTCF is required for the formation of specific loop anchors and distinct borders between TADs. To test these hypotheses further, we analyzed whether and how genome structure is altered in WAPL-depleted cells, in which cohesin cannot be properly released from DNA (Tedeschi *et al*, 2013). We were also interested in understanding how WAPL depletion causes mild chromatin compaction and accumulation of cohesin in axial structures (“vermicelli”), and we wanted to know whether and how WAPL’s binding partners PDS5A and PDS5B contribute to these processes.

To address these questions, we first depleted WAPL, PDS5A, and PDS5B (in the figures abbreviated as W, A, and B, respectively) either singly or in combination and analyzed cohesin distribution and chromatin morphology in fixed cells. For this purpose, we used HeLa cells in which all SCC1 alleles were modified to encode SCC1-mEGFP (Fig 1A and B) (Davidson *et al*, 2016), enabling us to analyze endogenous functional cohesin. Because of the large number of possible combinations in which WAPL, PDS5A, and PDS5B could be depleted, we used RNA interference (RNAi) instead

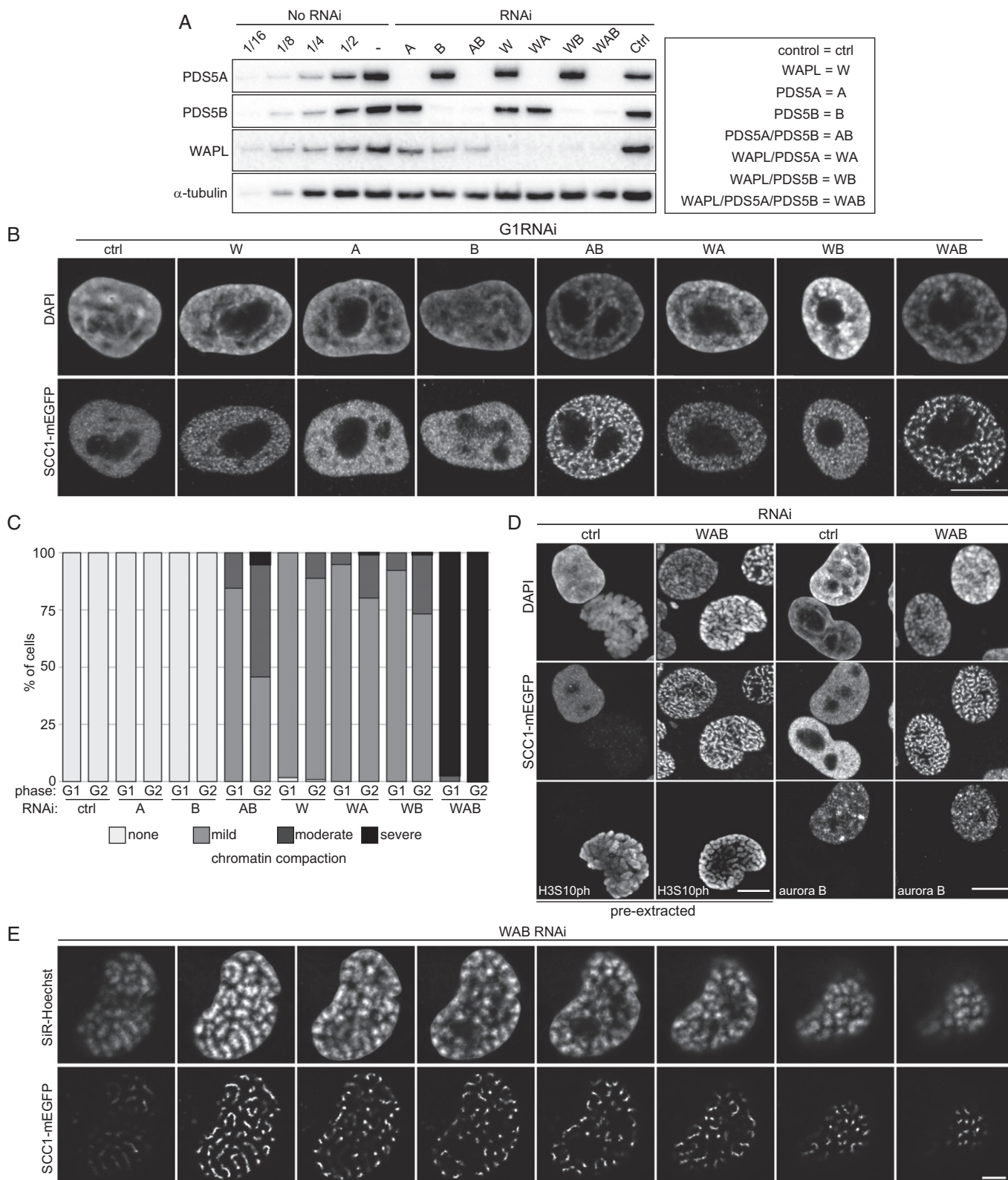


Figure 3.

of AID tagging in these experiments. Immunoblot analyses indicated that RNAi enabled depletion efficiencies of > 88% for PDS5B and > 94% for PDS5A and WAPL (Fig 3A).

Immunofluorescence microscopy revealed that WAPL depletion caused accumulation of SCC1 in vermicelli, as previously seen in mouse embryonic fibroblasts (MEFs) (Tedeschi *et al*, 2013;

Figure 3. Depletion of PDS5A/B induces chromatin compaction and vermicelli formation.

- A Immunoblotting analysis of SCC1-mEGFP cells treated with indicated single siRNAs or their combinations.
 B Representative immunofluorescence images of SCC1-mEGFP cells shown in (A) stained for GFP at G1-phase. DNA was counterstained with DAPI. Scale bar indicates 10 μm .
 C Phenotypic classification of chromatin compaction in G1- and G2-phase in (B) and Appendix Fig S2, $n > 100$ cells per condition.
 D Immunofluorescence microscopy of SCC1-mEGFP cells depleted for WAB or control-depleted (ctrl). Fixed cells with or without pre-extraction were stained for GFP and DAPI in combination with either phospho-H3 Ser10 (H3S10ph) or aurora B staining. Scale bar indicates 10 μm .
 E Live-cell imaging of SCC1-mEGFP cells depleted for WAB. Individual confocal sections from Appendix Fig S2D are shown, using 0.4 μm confocal distance between original sections. DNA was counterstained with SiR-DNA. Scale bar indicates 5 μm .

Source data are available online for this figure.

Busslinger *et al*, 2017). In contrast, depletion of PDS5A or PDS5B had little effect on cohesin localization, and co-depletion of WAPL with either PDS5A or PDS5B did not enhance the vermicelli phenotype seen after depletion of WAPL alone. However, co-depletion of PDS5A and PDS5B caused accumulation of cohesin in vermicelli (Fig 3B), as recently also reported by (Ouyang *et al*, 2016). Vermicelli in cells depleted of both PDS5 proteins were more pronounced than after WAPL depletion, and simultaneous depletion of all three proteins enhanced this phenotype even further (Fig 3B).

Staining of DNA with 4',6-diamidino-2-phenylindole (DAPI) revealed that WAPL depletion and co-depletion of PDS5A and PDS5B caused mild chromatin compaction, as seen in WAPL-depleted MEFs (Tedeschi *et al*, 2013). However, depletion of all three proteins caused strong condensation, resulting in the separation of chromatin into individual chromosomes (Fig 3B and C; Appendix Fig S2A). These were in many cases as condensed as chromosomes in mitotic prophase, even though cells depleted of WAPL, PDS5A, and PDS5B remained in interphase, as judged by the absence of histone H3 phosphorylated on serine 10 (H3S10ph; Fig 3D). Instead, co-staining with aurora B antibodies revealed that the cohesin localization and chromatin compaction phenotypes were present in both G1-phase (aurora B negative) and G2-phase (aurora B positive; Fig 3D), with slightly higher penetrance in G2 (Fig 3C and Appendix Fig S2B). Similar phenotypes were observed by live-cell imaging, ruling out fixation artifacts (Appendix Fig S2C). Confocal live-cell imaging showed that condensed chromosomes tended to be localized near the nuclear periphery (Fig 3E and Appendix Fig S2D), as are chromosomes in prophase.

These results indicate that, like WAPL, PDS5 proteins control cohesin localization and chromatin compaction, that the functions of PDS5A and PDS5B in these processes are redundant, and that depletion of all three proteins causes compaction of chromatin to a remarkably strong extent, as is normally only seen in early mitosis.

Co-depletion of PDS5 proteins increases the residence time and amounts of cohesin on chromatin

WAPL depletion increases the residence time and amounts of cohesin on interphase chromatin (Kueng *et al*, 2006; Tedeschi *et al*, 2013). We therefore analyzed if depletion of PDS5 proteins has similar effects. Consistent with a recent report (Ouyang *et al*, 2016), inverse fluorescence recovery after photobleaching (iFRAP) experiments, performed in cells synchronized in G1-phase, showed that

co-depletion of PDS5A and PDS5B increased the chromatin residence time of cohesin significantly to $t_{1/2} = 12.2$ min, compared to 4.8 min in control cells (Fig 4A and B). However, co-depletion of PDS5 proteins stabilized cohesin less on chromatin than depletion of WAPL ($t_{1/2} = 28.9$ min) or depletion of all three proteins ($t_{1/2}$ could not be measured in these cells due to the slow recovery of cohesin; Fig 4C). Despite these differences, co-depletion of PDS5A and PDS5B caused accumulation of cohesin on chromatin to a similar extent as was seen after WAPL depletion, both in quantitative IFM experiments (Fig 4D–F) and in chromatin fractionation experiments in which samples were analyzed by immunoblotting (Fig 4G). In both assays, the increase in cohesin on chromatin was small, presumably because approximately 50% of cohesin is already bound to chromatin in control cells (Gerlich *et al*, 2006). Inactivation of cohesin release can therefore maximally lead to a twofold increase in cohesin on chromatin. This is difficult to detect by immunoblotting (compare lanes 7 and 10–12 in Fig 4G) but can be inferred from the loss of cohesin from supernatant fractions (compare lanes 13 and 16–18).

These results indicate that both PDS5 proteins cooperate with WAPL in releasing cohesin from chromatin and that WAPL has a more important role in this process, as its depletion increases cohesin's residence time much more than depletion of PDS5 proteins (Fig 4B). However, the precise contribution of the different proteins is difficult to assess from RNAi experiments because these tend to cause hypomorphic conditions and not “null” phenotypes.

No evidence that condensin complexes contribute to chromosome condensation in cells depleted of WAPL and PDS5 proteins

Because simultaneous depletion of WAPL and PDS5 proteins causes mitotic-like condensation of chromosomes, we analyzed the localization and function of condensin complexes, which have been implicated in mitotic chromosome condensation. For this purpose, we used HeLa cells in which all alleles of either CAP-D2 or CAP-D3 were modified to encode C-terminal mEGFP fusion proteins, enabling the visualization of endogenous condensin I and condensin II complexes, respectively (Fig EV3A). Whereas co-depletion of WAPL and PDS5 proteins caused the re-localization of cohesin into vermicelli as described above, no change in condensin localization could be detected, with condensin I remaining cytoplasmic and condensin II remaining evenly distributed in the nucleus (Fig EV3B). Furthermore, co-depletion of SMC2, a subunit of both condensin I and II (Ono *et al*, 2003; Yeong *et al*, 2003), together with WAPL, PDS5A, and PDS5B did

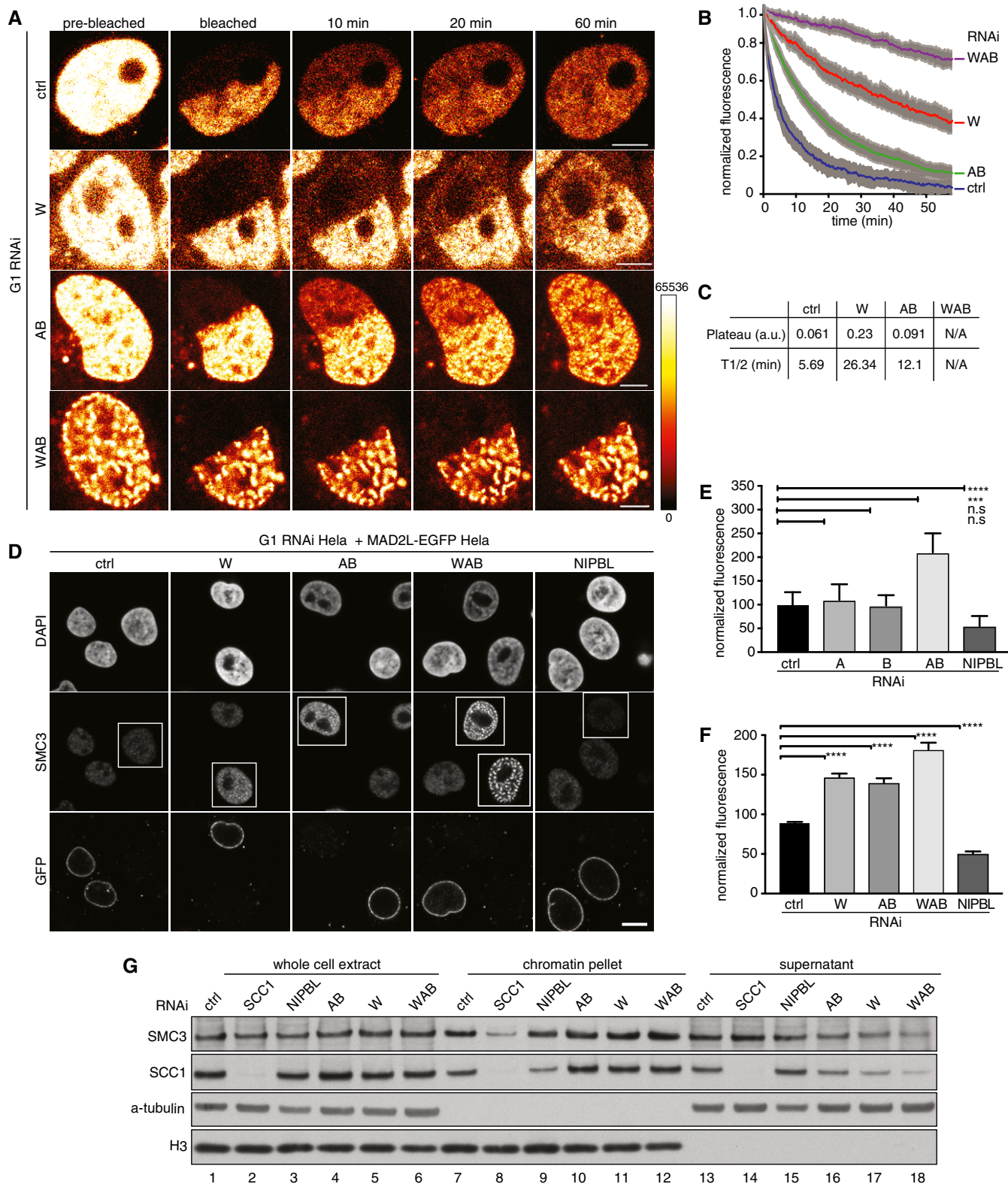


Figure 4.

not prevent chromosome condensation and vermicelli formation (Fig EV3C and D). These results do not formally exclude a role for condensins because they may not have been fully depleted by

RNAi, but they do imply that cohesin is the major cause of chromosome condensation in cells depleted of WAPL, PDS5A, and PDS5B.

Figure 4. RNAi depletion of PDS5A/B increases the amount and residence time of chromatin-bound cohesin.

- A Representative images of an inverse fluorescence recovery after photobleaching (iFRAP) experiment using SCC1-mEGFP cell lines in G1-phase that were control-depleted (ctrl) or depleted for WAPL (W), PDS5A/B (AB), WAPL/PDS5A/B (WAB). Fluorescence intensities are false-colored as indicated. Scale bar indicates 5 μ m.
- B Normalized signal intensities after photobleaching, for the iFRAP experiment shown in (A). Error bars denote standard error of the mean (s.e.m.), $n > 8$ cells per condition.
- C Quantification of the plateau and half-life of recovery for the curves in (B). a.u. indicates arbitrary unit.
- D Immunofluorescence staining of chromatin-bound SMC3 in HeLa cells. HeLa cells were control-depleted (ctrl) or depleted for WAPL (W), PDS5A/B (AB), WAPL/PDS5A/B (WAB), or NIPBL, mixed and seeded with HeLa cells expressing MAD2L-EGFP. RNAi treated cells are entangled. These cells were pre-extracted prior to fixation and stained for DAPI, SMC3, and GFP. Scale bar indicates 10 μ m.
- E Quantification of SMC3 fluorescence intensities obtained in the experiments shown in (D). SMC3 fluorescence intensities were normalized to those of neighboring RNAi-untreated cells expressing MAD2L-EGFP. The asterisk denotes a significant difference according to a Dunn's-corrected Kruskal–Wallis test ($n > 90$, **** P -value ≤ 0.0001 , *** P -value ≤ 0.001 , N.S. = P -value > 0.05). Error bars denote standard error of the mean (s.e.m.).
- F Same as panel (E) except for using PDS5A-mEGFP cell lines as RNAi-untreated cells. The asterisk denotes a significant difference according to a Dunn's-corrected Kruskal–Wallis test ($n > 30$, **** P -value ≤ 0.0001). Error bars denote standard error of the mean (s.e.m.).
- G Immunoblotting analysis of the whole-cell extract, the chromatin pellet fraction and the supernatant fraction from HeLa cells treated with siRNAs indicated on the left.

Source data are available online for this figure.

Depletion of WAPL, PDS5A, and PDS5B weakens compartments but increases the size of TADs

To understand how depletion of WAPL and PDS5 proteins causes vermicelli formation and chromatin compaction, we performed Hi-C experiments. For this purpose, we depleted WAPL alone, or PDS5A and PDS5B together, or all three proteins in cells synchronized in G1-phase and compared them to cells transfected with control siRNAs. For comparison, we also analyzed cells not transfected with siRNAs which had been synchronized in S-phase, G2-phase, or prometaphase (see below). All Hi-C experiments were performed as independent biological replicates. Cell samples from the same populations that were used in Hi-C experiments were analyzed for DNA content by fluorescence-activated cell-sorting (FACS), DNA replication by EdU incorporation, G1 versus G2 distribution by aurora B staining, and for chromatin morphology and cohesin localization by DAPI and SCC1 staining, respectively (Fig 5A). Results from the Hi-C biological replicates were highly consistent (Table EV1 and Appendix Fig S3), and the low frequency of inter-chromosomal interactions, only representing 1.5% for prometaphase and between 4–6% for all other Hi-C libraries, was indicative of high-quality datasets (Table EV1).

Coverage-corrected Hi-C contact matrices in cells depleted of WAPL, PDS5A, and PDS5B, and all three proteins showed increasing similarities to matrices from prometaphase cells (Fig 5B and Appendix Fig S3A and see below). Compared to control G1 cells, contact frequencies were reduced in the 50–250 kb range but increased in the 0.4–2.5 Mb range, with a peak around 600–700 kb in cells depleted of WAPL or PDS5A and PDS5B, and around 1.1 Mb in cells depleted of all three proteins (Fig 5C and D; Appendix Fig S3B and C).

Compartmentalization was reduced in cells depleted of WAPL, PDS5A, and PDS5B, or all three proteins, with WAPL-depleted cells showing the weakest and triply depleted cells showing the strongest reduction (Fig 6A and Table EV1). The compartment signal derived by eigenvector analysis from Hi-C data confirmed this, as the pattern of alternating A and B compartments observed in control cells was partially lost following depletion of either WAPL or PDS5A and PDS5B, and was even more strongly reduced in triply depleted cells (Fig 6A, top panels above the Hi-C maps). The

compartment signals became weaker genome-wide, as could be seen by linearly fitting the signals detected in experimental cells to those obtained in G1 control cells. This resulted in slope values of 0.5, 0.34, and 0.26 for cells depleted of WAPL, PDS5A, and PDS5B, or all three proteins, respectively (Fig 6B), confirming that WAPL depletion reduces compartmentalization the least and depletion of all three proteins the most. A strong reduction in compartmentalization was also seen in genome-wide aggregate contact enrichment analyses of 50 compartment categories (Fig 6C).

Whereas compartmentalization was reduced in cells depleted of WAPL, PDS5A, and PDS5B, strikingly, many TADs were larger in size than in control cells (Fig 7A; contacts detected in the indicated experimental conditions are shown in the upper right halves of the spilt Hi-C maps; TADs called by Homer software are indicated; contacts that are specifically occurring in the experimental conditions but not in G1 control cells are shown as difference maps in the lower left halves). Whereas in control cells only relatively few interactions outside of TADs could be observed, these became more prominent in cells depleted of WAPL, PDS5A, and PDS5B. This was also observed using aggregate TAD analysis (Fig EV4A). New long-range contacts could be seen emerging from existing loops (see below), but also from “ordinary” (or non-loop) TADs (Rao *et al*, 2014). Among 826 TADs that clearly represented “ordinary domains,” we found 344 from which new long-range contacts emerged. This increase in inter-TAD contact frequencies (and, at the same time, a relative decrease of intra-TAD contact frequencies) resulted in the partial fusion of typically two or three TADs into one. This phenomenon resulted in a decrease in TAD numbers (Fig 7B), an increase in TAD size (Fig 7C), and a reduction in the insulation (Fig 7D) and directionality bias (Fig EV4B) between TADs at relatively constant genome coverage by TADs (Table EV1). These effects were weakest in cells depleted only of WAPL and most pronounced in cells depleted of all three proteins.

We confirmed these results by performing Hi-C experiments in quiescent MEFs from which the *Wapl* gene had been deleted (Tedeschi *et al*, 2013). In these cells, as in HeLa, we observed a genome-wide shift toward long-range contacts (Fig 8A and B), weakening of compartments, increased local long-range interactions (Fig 8C and D; new long-range contacts emerged from 333 out of 658 TADs which were unambiguously identified as “ordinary

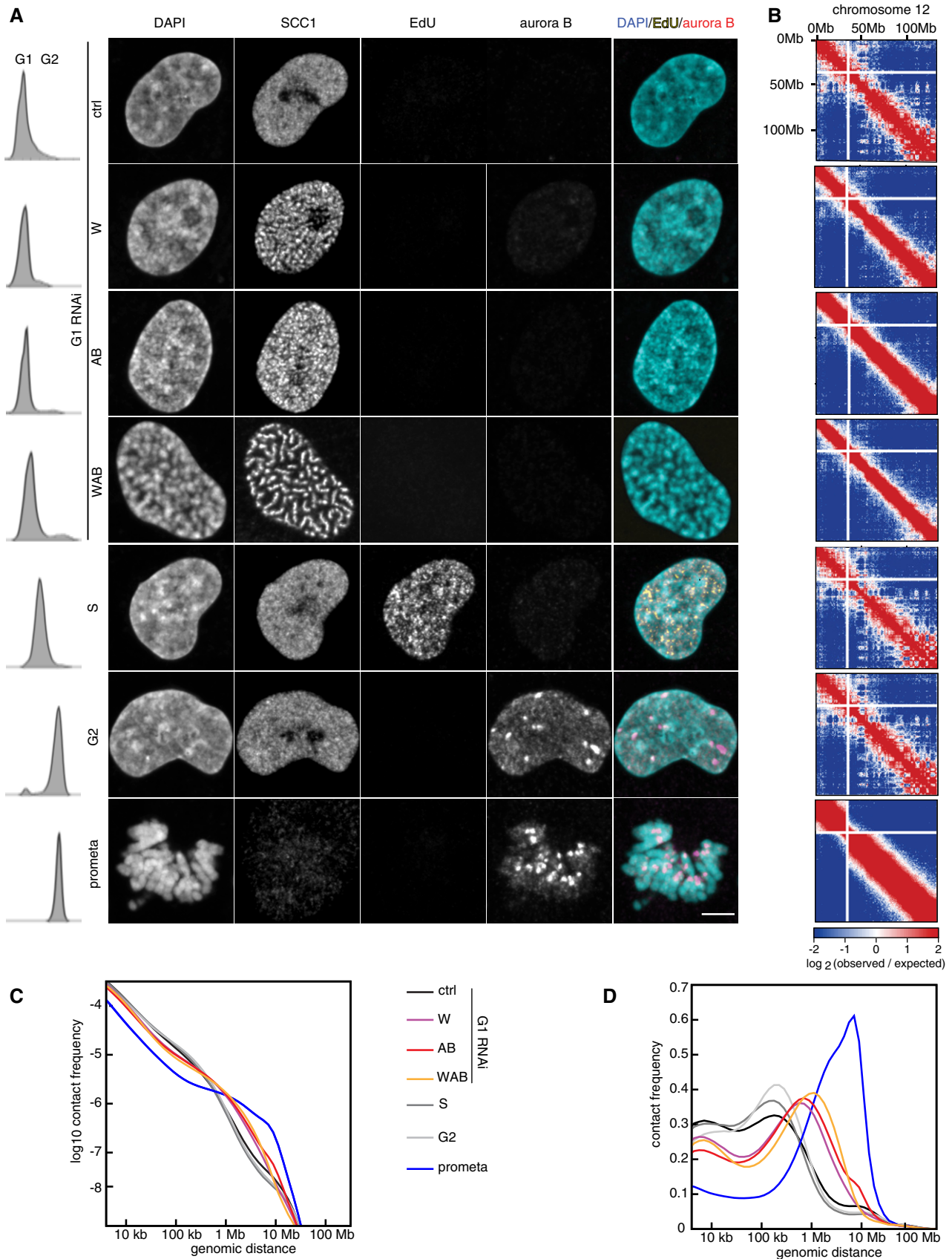


Figure 5.

Figure 5. Hi-C of WAPL and PDS5A/B RNAi depletion shows longer-range contacts.

- A Immunofluorescence staining of DAPI, SCC1, EdU, aurora B, and joint DAPI/EdU/aurora B staining (from left to right) for control G1-phase (ctrl), WAPL-depleted (W), PDS5A/PDS5B-depleted (AB), joint WAPL/PDS5A/PDS5B-depleted (WAB), S-phase (S), G2-phase (G2), and prometaphase (prometa) cells (from top to bottom) together with flow-cytometry profiles on the left. Scale bar indicates 5 μ m.
- B Coverage-corrected Hi-C contact enrichment matrices (using HOMER) of chromosome 12, for the same conditions as in (A).
- C, D Intra-chromosomal contact frequency distribution as a function of genomic distance using equal sized (C) or logarithmically increasing (D) genomic distance bins, for control G1-phase (ctrl, black), WAPL-depleted (W, purple), PDS5A/PDS5B-depleted (AB, red), joint WAPL/PDS5A/PDS5B-depleted (WAB, yellow), S-phase (S, dark gray), G2-phase (G2, light gray) and prometaphase (prometa, blue) cells.

domains”) and a reduced TAD boundary strength as seen by changes in directionality index (Fig 8E) and insulation score (Fig 8F). These observations rule out the possibility, at least for WAPL-depleted cells, that the results obtained in HeLa cells are biased by the abnormal karyotype of these cells.

At variance with our results, Haarhuis *et al* (2017) reported during preparation of our manuscript that WAPL depletion does not cause a reduction in TAD boundary strength. However, re-analysis of their data with the same algorithms used in our study (Appendix Fig S4) revealed some weakening of TAD boundary strength also in their data, although not to the same extent as seen in ours, both using directionality index (Appendix Fig S4A) and insulation score measurements (Appendix Fig S4B). This implies that differences between their and our results are caused at least in part by differences in the bioinformatic analyses.

These results indicate that depletion of WAPL, PDS5A, and PDS5B suppresses A and B compartments and enables the formation of long-range interactions that extend beyond the borders of TADs as they occur in control cells, resulting in the partial fusion of TADs.

An alternative interpretation of our data could be that WAPL depletion leads to loss of local compaction without affecting higher-order organization of TADs. This is a formal possibility because the observed contact frequencies reflect their relative abundance, and a decrease in short-range contacts from a particular locus would therefore also result in an increase of long-range contacts, and *vice versa*. However, we consider this interpretation less plausible because it could not explain the strong chromatin compaction phenotypes we observed in these cells and the simulations reported by the Mirny lab (Fudenberg *et al*, 2016).

Chromatin looping is altered differently following depletion of WAPL and PDS5 proteins

Interestingly, close inspection of the interaction matrices revealed that point interactions such as those at the corners of TADs were altered differently upon depletion of WAPL and PDS5 proteins (Fig 9; for examples of point interactions called by “juicer-tool”, see lower left half of the split Hi-C matrices in Fig 9A, marked by small black dots).

In WAPL-depleted cells, both the number of these loops and their length were increased from 10,310 in control cells (median length 262.5 kb) to 14,557 (median length 387.5 kb; Fig 9B and C; note that in this experiment, more loops could be identified than in Appendix Fig S1C because more replicates were analyzed). Following WAPL depletion, more of the looping loci (loop anchors) participated in multiple interactions (55.4%) than in control cells (40.7%; Appendix Fig S5A, left panel), resulting in “chains” and “networks” of loops (examples of loop networks can be seen in Fig 9A in the second panel from the top as parallel chains of dots). In the case of

networks, 21.6% of these contained at least 10 loops in WAPL-depleted cells, compared to only 6.4% in control cells (Appendix Fig S5A, right panel). However, aggregate loop analysis revealed that, on average, the loops specifically detected in WAPL-depleted cells also existed in control cells, albeit below the detection threshold (Fig 9D, top two panels). In contrast, WAPL depletion did not strengthen the contact enrichment of the looping loci that were already above detection threshold in control cells (Fig 9E, top four panels). These observations indicate that the loops that can be detected specifically in WAPL-depleted cells are formed by extension of shorter loops that are also present in control cells, and that the extended loops in WAPL-depleted cells also exist in control cell populations, but at much lower frequencies. In other words, the same set of interactions exist in control and WAPL-depleted cells, but long-range interactions are much more frequent after WAPL depletion.

Unexpectedly, loops were affected differently in cells in which both PDS5 proteins were depleted. These contained many fewer loops than control cells, both when depleted alone (5,893) or when co-depleted with WAPL (5,259; Fig 9B), and the contact enrichment of looping loci that were present in control cells were weakened (Fig 9E, panels in third and fourth rows). This is surprising given that genome-wide, contact frequencies were altered very similarly in cells depleted of WAPL and of PDS5 proteins (Fig 5C and D; Appendix Fig S3B and C). The situation in cells depleted of PDS5 proteins is, therefore, reminiscent of the situation in CTCF-depleted cells, in which loop numbers are also greatly reduced, whereas interaction frequencies at the genomic level remain unchanged (Fig 2F and K). This similarity raises the interesting possibility that PDS5 proteins are required for the boundary function of CTCF (see Discussion).

Loops specifically detected in cells depleted of PDS5 proteins and WAPL “violate” the CTCF convergence rule

Remarkably, depletion of PDS5 proteins also led to a strong violation of the CTCF convergence rule (Fig 9F). To be able to determine this, we performed chromatin immunoprecipitation-sequencing experiments (ChIP-seq) to identify the genomic distribution of cohesin and CTCF in control cells, and in cells depleted of WAPL, or PDS5A and PDS5B, or all three proteins (Appendix Fig S5D and E). To analyze the orientation of CTCF sites at loop anchors, we identified contacts that overlapped with both cohesin (SMC3) and CTCF ChIP-seq peaks and had a consensus CTCF binding motif. In control cells, 73.8% of loops fulfilling these criteria were anchored at convergent CTCF sites, whereas many fewer had been formed between tandemly oriented (24.7%) and divergent (1.5%) sites (Fig 9F), confirming previous reports (Rao *et al*, 2014; Vietri Rudan *et al*, 2015). However, of the loops that fulfilled these criteria and were specifically detected in cells depleted of PDS5A and PDS5B (i.e., not detectable in control cells), only 30.9% were anchored by

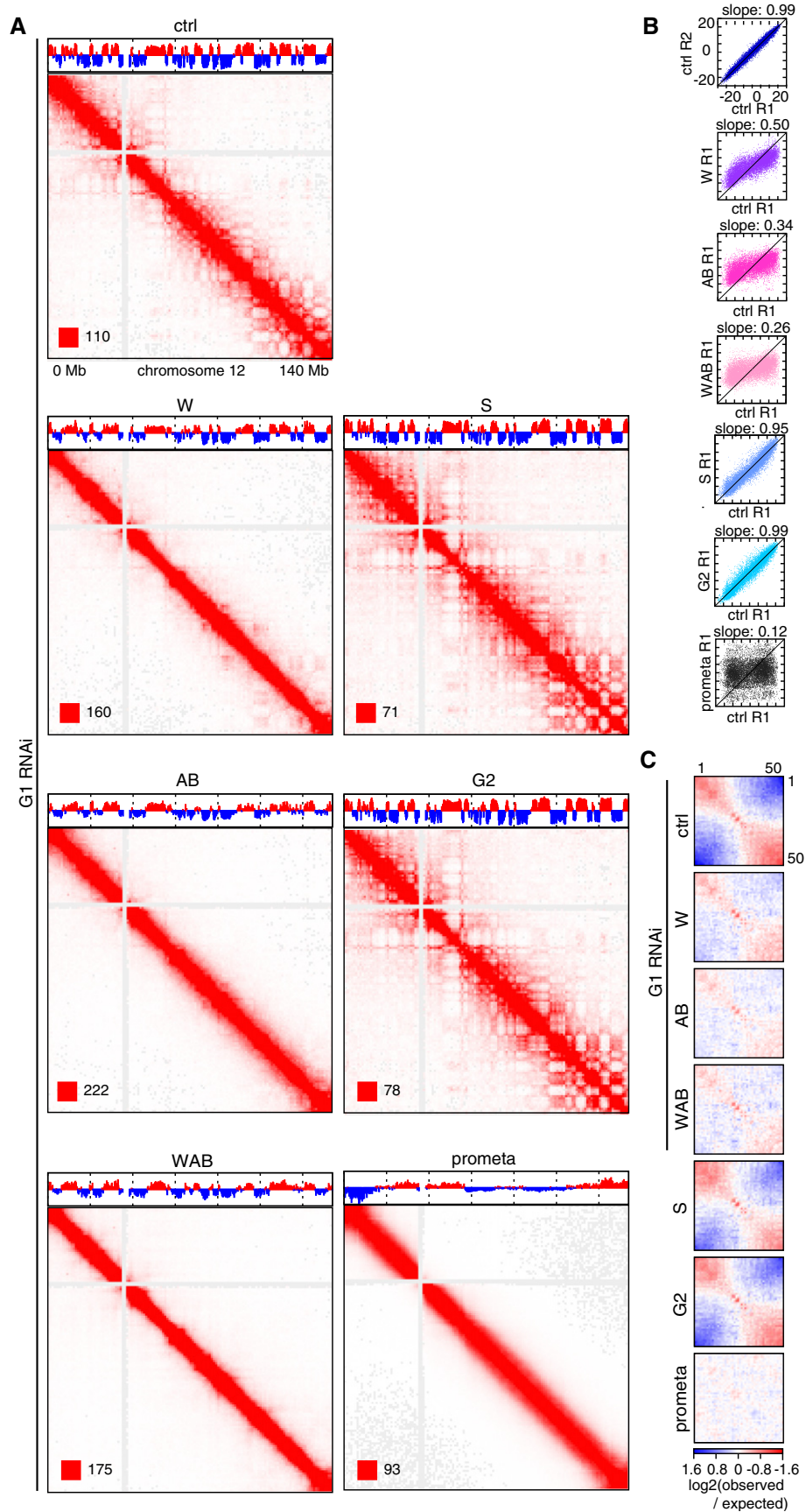


Figure 6.

Figure 6. Compartmentalization weakens upon WAPL and PDS5A/B RNAi depletion.

- A Coverage-corrected Hi-C contact matrices of chromosome 12, for control-depleted (ctrl), WAPL-depleted (W), PDS5A/PDS5B-depleted (AB), joint WAPL/PDS5A/PDS5B-depleted (WAB) cells in G1-phase, as well as S-phase (S), G2-phase (G2), and prometaphase (prometa) cells. The corresponding compartment signal tracks at 250 kb bin resolution are shown above the matrices. The matrices were plotted using Juicebox.
- B Scatter plots of compartment signal values at 250 kb bin resolution, in the second replicate of control-depleted G1-phase cells (ctrl R2) and the first replicates (R1) of the other conditions (vertical axes) compared to the first replicate of control-depleted G1-phase cells (ctrl R1, horizontal axis). The slope of the linear fit is shown above the plots, and $x = y$ (slope = 1) is drawn as black lines.
- C Inter-chromosomal contact enrichment between genomic bins with varying compartment signal strength from most B-like (1) to most A-like (50), for the same conditions as in (A).

convergent CTCF sites. Instead, most of these loops (54.5%) were anchored by tandemly oriented CTCF sites, and many more than normally by divergent sites (14.6%). This distribution is much more like what would be expected if CTCF sites were oriented randomly at loop anchors (25% convergent, 50% tandem, 25% divergent) than like the distribution seen in control cells.

An even more randomized distribution of CTCF site orientations was observed at the anchors of loops specifically detected in cells co-depleted of both PDS5 proteins and WAPL (30.4% convergent, 51.5% tandem, and 18.1% divergent), whereas loops specifically detected in cells depleted of WAPL alone violated the convergence rule to a lesser extent (49.8% convergent, 44.7% tandem, and 5.5% divergent, Fig 9F). Interestingly, in the “chains” of loops, in which the upstream anchor of a loop is also the downstream anchor of a consecutive loop of the chain, the CTCF convergence rule was more frequently violated by internal loops than by the loops which were formed by the outmost anchors (Appendix Fig S5B). This contrast was particularly strong in WAPL-depleted cells, while remarkably, after depletion of PDS5 proteins alone or together with WAPL, the CTCF convergence rule was also violated in the loops formed by the outmost anchors.

These results indicate that in cells depleted of PDS5 proteins and WAPL, CTCF boundaries can be skipped more frequently than normally, and that loops which are not anchored by convergent CTCF sites can be formed much more frequently.

We also used the cohesin ChIP-seq data to analyze whether the disappearance of loops in cells depleted of WAPL and PDS5 proteins coincides with changes in cohesin localization. We found that this was indeed the case (Appendix Fig S5D and E). For example, we identified 7,197 sequences which functioned as loop anchors in control cells but not in cells depleted of WAPL, PDS5A, and PDS5B. These sequences contained 6,321 cohesin peaks in control cells, of which 1,788 (28.3%) disappeared in cells depleted of WAPL and PDS5 proteins, whereas 728 new cohesin peaks appeared in these cells. Some cohesin ChIP-seq peaks also disappeared from regions which still functioned as loop anchors in cells depleted of WAPL and PDS5 proteins, but many fewer than in regions that had lost their looping functions (Appendix Fig S5E). These results further support the notion that chromatin loops are mediated by cohesin and they indicate that depletion of WAPL and PDS5 proteins changes long-range chromatin interactions by altering the distribution of cohesin on DNA.

The effects of WAPL, PDS5A, and PDS5B depletion on chromatin structure depend on cohesin and are rapidly reversible

To test whether chromosome condensation and altered genomic interactions in cells depleted of WAPL, PDS5A, and PDS5B depend

on cohesin, we generated cells in which chromatin could be imaged while cohesin was inactivated by auxin-mediated degradation. For this purpose, we stably expressed the histone H2B fused to mRaspberry in SCC1-mEGFP-AID cells, co-depleted WAPL, PDS5A, and PDS5B by RNAi, and subsequently induced SCC1 degradation (Fig 10A). Under these conditions, in which most cohesin is bound to chromatin, SCC1-mEGFP-AID was degraded rapidly in 20 min, leading to the disappearance of vermicelli (Fig 10A, right panel). Interestingly, chromosomes de-condensed concomitant with cohesin degradation. Quantification of this phenomenon by automated image segmentation revealed that chromosomes began to de-condense rapidly during the initial 10–20 min, that is, when cohesin degradation occurred, but continued to expand at a slower rate for at least 60 min (Fig 10B, right panel).

To analyze chromatin structure, we performed Hi-C experiments after auxin treatment for 0, 15, and 180 min (Fig 10C–F). Corroborating our results reported above, depletion of WAPL, PDS5A, and PDS5B strongly suppressed compartmentalization but increased the size of TADs. However, addition of auxin reverted these phenotypes, leading after 180 min to interaction matrices that were like those seen in cells partially depleted of cohesin, that is, compartments were strengthened (Fig 10C and D), whereas loops and TADs were weakened (Fig 10E and F, Appendix Fig S5F).

These results indicate that the strong chromosome condensation seen in cells co-depleted of WAPL, PDS5A, and PDS5B depends on cohesin, as does the mild chromatin compaction caused by WAPL depletion in MEFs (Tedeschi *et al*, 2013). Furthermore, these experiments show that the suppression of compartmentalization and the weakening of TAD insulation in cells depleted of WAPL, PDS5A, and PDS5B depend on cohesin, and interestingly, they raise the possibility that cohesin inactivation affects different steps of chromosome de-condensation with different kinetics.

Chromatin structure changes in WAPL-, PDS5A-, and PDS5B-depleted cells are similar but not identical to changes that occur during mitotic chromosome condensation

Because co-depletion of WAPL, PDS5A, and PDS5B resulted in chromatin condensation reminiscent of that observed in prophase (Fig 3), we compared the Hi-C interaction matrices of these cells with those of cells synchronized in different cell cycle stages, including prometaphase (Fig 5).

A comparison of the different stages showed overall similar genome-wide interaction frequencies in G1, S, and G2, with a small increase in short-range interactions (60–800 kb) and a corresponding decrease in long-range interactions (3–30 Mb) in cells in S and G2 relative to G1 (Fig 5C and D). Furthermore,

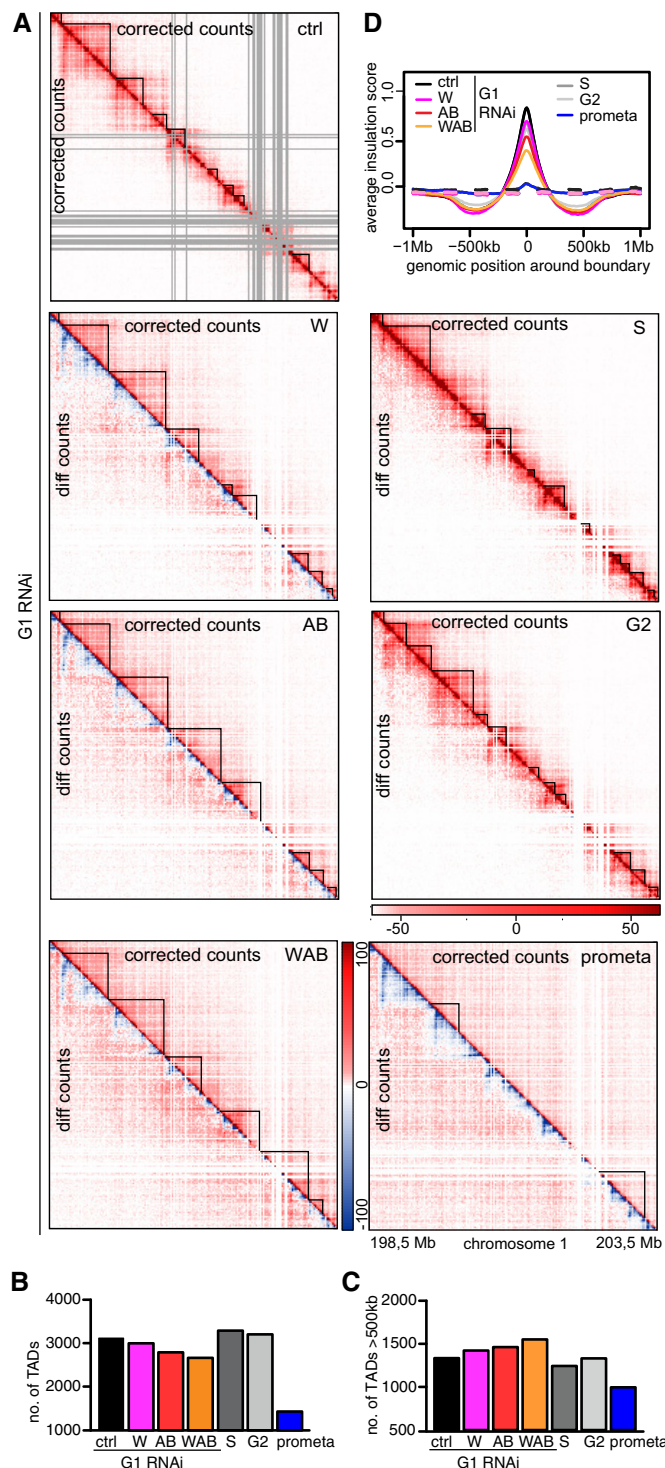


Figure 7. TAD boundaries weaken upon WAPL and PDS5A/B RNAi depletion.

A Coverage-corrected Hi-C contact count matrices (upper triangles, using HOMER) in the 198.5–203.5 Mb region of chromosome 1, for control-depleted (ctrl), WAPL-depleted (W), PDS5A/PDS5B-depleted (AB), joint WAPL/PDS5A/PDS5B-depleted (WAB) cells in G1-phase, as well as S-phase (S), G2-phase (G2), and prometaphase (prometa) cells. Contact count difference matrices compared to ctrl-G1 (lower triangles) are shown for all non-control conditions.

B, C The number of TADs (B) and the number of long (> 500 kb) TADs (C) in the same conditions as in (A). Colors are as in Fig 5C.

D Average insulation score around TAD boundaries identified in control-depleted G1 cells, for the same conditions as in (A). Dashed lines show the average insulation score around the +1 Mb shifted boundaries as control.

In contrast, in prometaphase cells, most interactions < 0.8 Mb were lost and long-range interactions (0.8–70 Mb) greatly increased, with 8–9 Mb interactions having the highest frequency (Fig 5C and D). Compartments could not be detected (Fig 6A–C), TADs were greatly reduced in number and size (Fig 7B and C), and almost all loops disappeared (Fig 9A–E; “juicer-tool” could only identify 57). These results confirm and extend previous analyses of cell populations in G1, S, and prometaphase (Naumova *et al*, 2013) and single-cell analyses of all four cell cycle stages (Nagano *et al*, 2017). We suspect that the fact that a relatively high number of TADs could still be called in Hi-C matrices from prometaphase cells (Table EV1 and Fig 7B), even though these were hardly detectable by visual inspection (Fig 7A) is due to the sensitivity of computational TAD detection (for further explanation, see Materials and Methods).

Interestingly, at two levels of genome organization, cells depleted of WAPL, PDS5A, and PDS5B were in an intermediate state between interphase and mitotic cells. Whereas in interphase and prometaphase cells, interactions were most frequently bridging distances of 0.3 and 8–9 Mb, respectively, in cells depleted of WAPL, PDS5A, and PDS5B the most frequent interactions occurred between loci 1–1.1 Mb apart (Fig 5C and D). Similarly, compartment “strength” was strongest in interphase cells (slope values of 0.95–0.99), weakest in prometaphase (slope value 0.12), and intermediate in cells depleted of WAPL, PDS5A, and PDS5B (slope values 0.26–0.5; Fig 6B). A similar trend was observed for the number of TADs, which decreased following depletion of WAPL, PDS5A, and PDS5B, that is, became more similar also in this respect to prometaphase cells (Fig 7B). These results indicate that depletion of WAPL, PDS5A, and PDS5B induces chromosome condensation by changes in genome organization that are similar to those occurring in mitosis, even though the former is caused by cohesin and the latter by condensin.

Discussion

Although cohesin was initially discovered as a protein complex essential for sister chromatid cohesion, it has long been suspected that cohesin has distinct roles in gene regulation and that it may be defects in these functions and not in cohesion that can contribute to tumorigenesis and lead to developmental defects, called cohesinopathies (reviewed in Watrin *et al*, 2016). It has also been realized

compartmentalization (Fig 6A–C) and position, number, size, and insulation of TADs (Fig 7A–D) were similar, whereas the number and length of loops decreased in S and increased again in G2, although not to the extent observed in G1 (Fig 9A–C). It will, therefore, be interesting to test whether DNA replication interferes with formation or maintenance of loops. As in G1, most loops formed between convergent CTCF sites in S and G2 (75.7 and 71.7%, respectively).

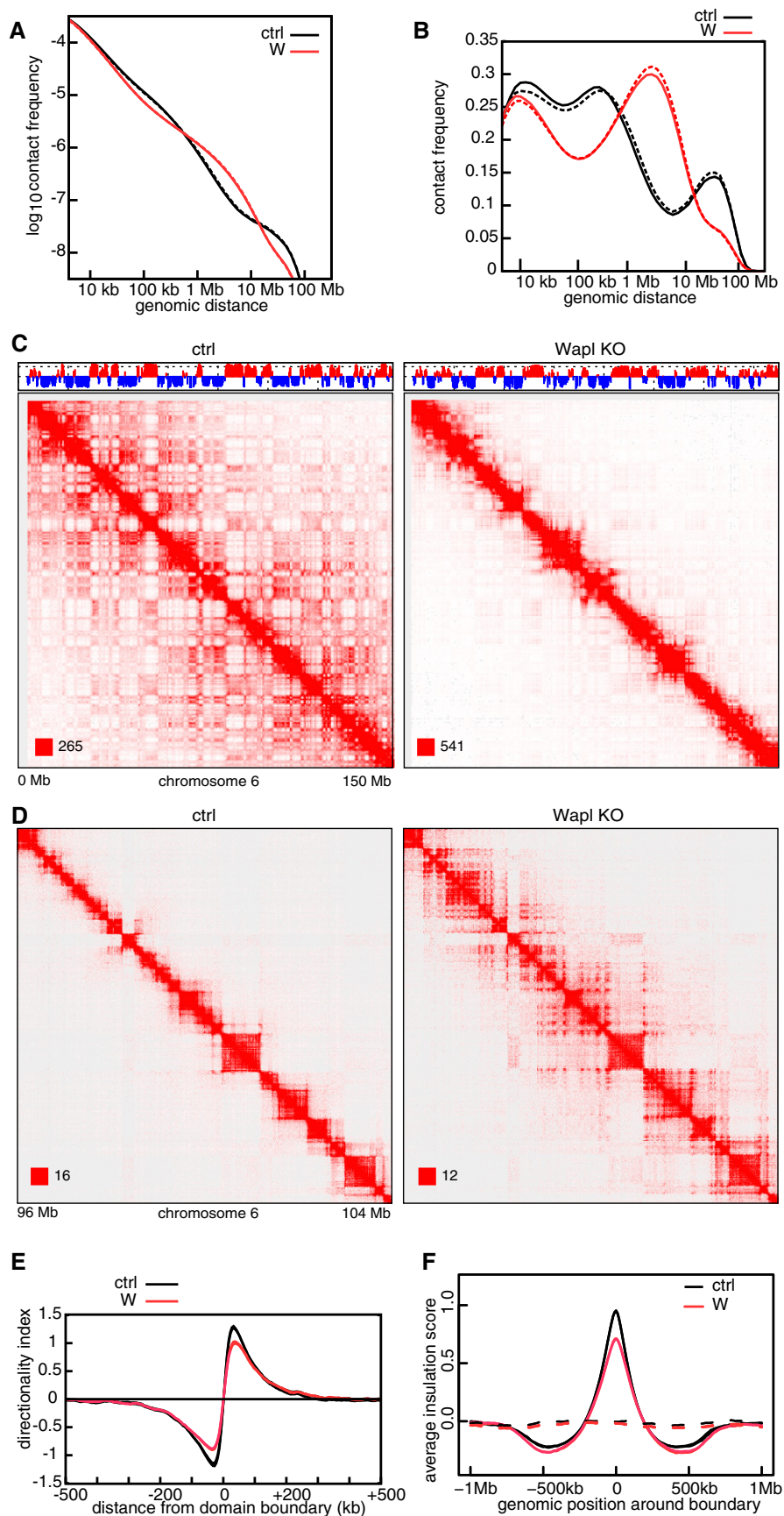


Figure 8.

Figure 8. Chromatin organization changes upon WAPL depletion in pMEFs.

- A, B Intra-chromosomal contact frequency distribution as a function of genomic distance using equal sized (A) or logarithmically increasing (B) genomic distance bins, for control (black) and Wapl KO (red) MEF cells. Solid and dashed lines show replicates.
- C Coverage-corrected Hi-C contact matrices of chromosome 6, in control (left) and Wapl KO (right) MEF cells. The corresponding compartment signal tracks at 250 kb bin resolution are shown above the matrices. The matrices were plotted using Juicebox.
- D For the same conditions, coverage-corrected Hi-C contact matrices in the 96–104 Mb region of chromosome 6, plotted by using Juicebox.
- E Average standardized directionality index profiles in a 1 Mb region centered around TAD boundaries identified in the control MEF cells, for the same conditions as in (A). Colors are as in (A).
- F Average insulation score around TAD boundaries identified in the control MEF cells, for the same conditions as in (A). Dashed lines show the average insulation score around the +1 Mb shifted boundaries as control. Colors are as in (A).

that cohesin's function in gene regulation is related to CTCF, as this DNA binding protein recruits cohesin to specific sites in mammalian genomes and depends on cohesin for its ability to mediate gene regulation (Parelho *et al*, 2008; Wendt *et al*, 2008; Buslinger *et al*, 2017). Because CTCF affects gene expression by chromatin looping (Kurukuti *et al*, 2006; Splinter *et al*, 2006), it has been speculated that CTCF and cohesin have discrete functions in chromatin organization, with CTCF specifying the genomic sites at which cohesin functions, and cohesin entrapping DNA sequences *in cis* to generate chromatin loops (Wendt *et al*, 2008; Wendt & Peters, 2009). This model predicts that chromatin loops depend on cohesin but not necessarily on CTCF, whereas conversely the identity of DNA sequences that form loop anchors would depend on CTCF but not on cohesin (Fig EV5B and C).

Earlier support for a role of cohesin in chromatin organization came from the observation that cohesin can compact chromatin when cohesin's residence time and levels are artificially increased on chromatin by depletion of WAPL (Tedeschi *et al*, 2013). However, whether cohesin is actually required for chromatin organization under physiological conditions has remained less clear as earlier cohesin inactivation experiments either only analyzed individual chromatin interactions (Hadjuri *et al*, 2009; Mishiro *et al*, 2009; Nativio *et al*, 2009) or did not reveal major changes in TADs and none in compartments (Seitan *et al*, 2013; Sofueva *et al*, 2013; Zuin *et al*, 2014; chromatin loops were not yet analyzed genome-wide in these studies). Our results reported here remove this uncertainty as they show clearly that TADs and loops are greatly weakened in the absence of cohesin. Our experiments further indicate that CTCF is not essential for long-range interactions *per se*, although we can formally not exclude that small amounts of CTCF persisted in our experiments and contributed to the chromatin interactions that were still detectable in CTCF-depleted cells. Our results show clearly, however, that CTCF is required for TAD insulation and the detectability of loops.

While cohesin had been predicted to mediate formation of TADs and loops, it was unexpected that cohesin depletion would increase the detectability of A and B compartments, which are thought to represent different compaction states of chromatin (euchromatin and heterochromatin, respectively) (Lieberman-Aiden *et al*, 2009; Rao *et al*, 2014). The notion that cohesin is a key determinant of chromatin structure, not only at the level of TADs and loops, but also at the level of compartments, is also supported by our observation that stabilization of cohesin on chromatin by WAPL depletion does not only increase the frequency with which cells can form long chromatin loops but also decreases the detectability of compartments. It will, therefore, be interesting to analyze whether cohesin-mediated long-range

interactions have a role in specifying euchromatic and heterochromatic regions.

We suspect that our results are at variance with previous cohesin and CTCF inactivation experiments in which only mild phenotypes could be detected (Seitan *et al*, 2013; Sofueva *et al*, 2013; Zuin *et al*, 2014; Kubo *et al*, 2017) because these proteins may have been depleted to various degrees in the different studies. This possibility is consistent with our observation that TAD patterns seem unaffected in SCC1-mEGFP-AID and CTCF-mEGFP-AID expressing cells if these are not treated with auxin (Appendix Fig S1D), even though the genome-wide analysis of chromatin interactions (Appendix Fig S1A) clearly indicates that these cells are hypomorphic for the roles of cohesin and CTCF in chromatin organization. It may be difficult to observe major changes in Hi-C experiments in which cohesin and CTCF were depleted incompletely, either because no calibration methods are presently available for Hi-C assays, and/or because small amounts of these proteins are sufficient for their function, as is known to be the case for the cohesion function of cohesin (Heidinger-Pauli *et al*, 2010).

Our results are, however, consistent with several other studies which were deposited on *bioRxiv* or published in peer-reviewed journals during preparation or after submission of our manuscript (Gassler *et al*, 2017; Haarhuis *et al*, 2017; Nora *et al*, 2017; Rao *et al*, 2017; Schwarzer *et al*, 2017). In these studies, chromatin structure was analyzed by Hi-C experiments following inactivation of either cohesin (Rao *et al*, 2017), the cohesin loading complex (Schwarzer *et al*, 2017), CTCF (Nora *et al*, 2017), or WAPL (Haarhuis *et al*, 2017). The results of these and our experiments, combined with the previous observations that cohesin and CTCF are enriched at TAD boundaries and loop anchors (Dixon *et al*, 2012; Rao *et al*, 2014), strongly support the hypothesis that cohesin is a key determinant of chromatin structure at multiple levels, that in the case of TADs and loops cohesin has a direct role in mediating long-range interactions, possibly by entrapping DNA sequences *in cis*, and that CTCF specifies where in the genome cohesin performs these functions.

Importantly, our results are also fully consistent with the loop extrusion hypothesis (Fig EV5A and Nasmyth, 2001; Sanborn *et al*, 2015; Fudenberg *et al*, 2016) based on which it had been predicted that WAPL depletion would lead to the formation of extended chromatin loops (Fudenberg *et al*, 2016). The fact that more and larger loops can indeed be detected in WAPL-depleted cells (Fig 9B and C and Haarhuis *et al*, 2017) and that these depend on cohesin (Fig EV5D) confirms this prediction and indicates that WAPL depletion causes chromatin compaction and accumulation of cohesin in axial positions (vermicelli) by loop extension. As had been pointed out (Fudenberg *et al*, 2016), the generation of these loops could be

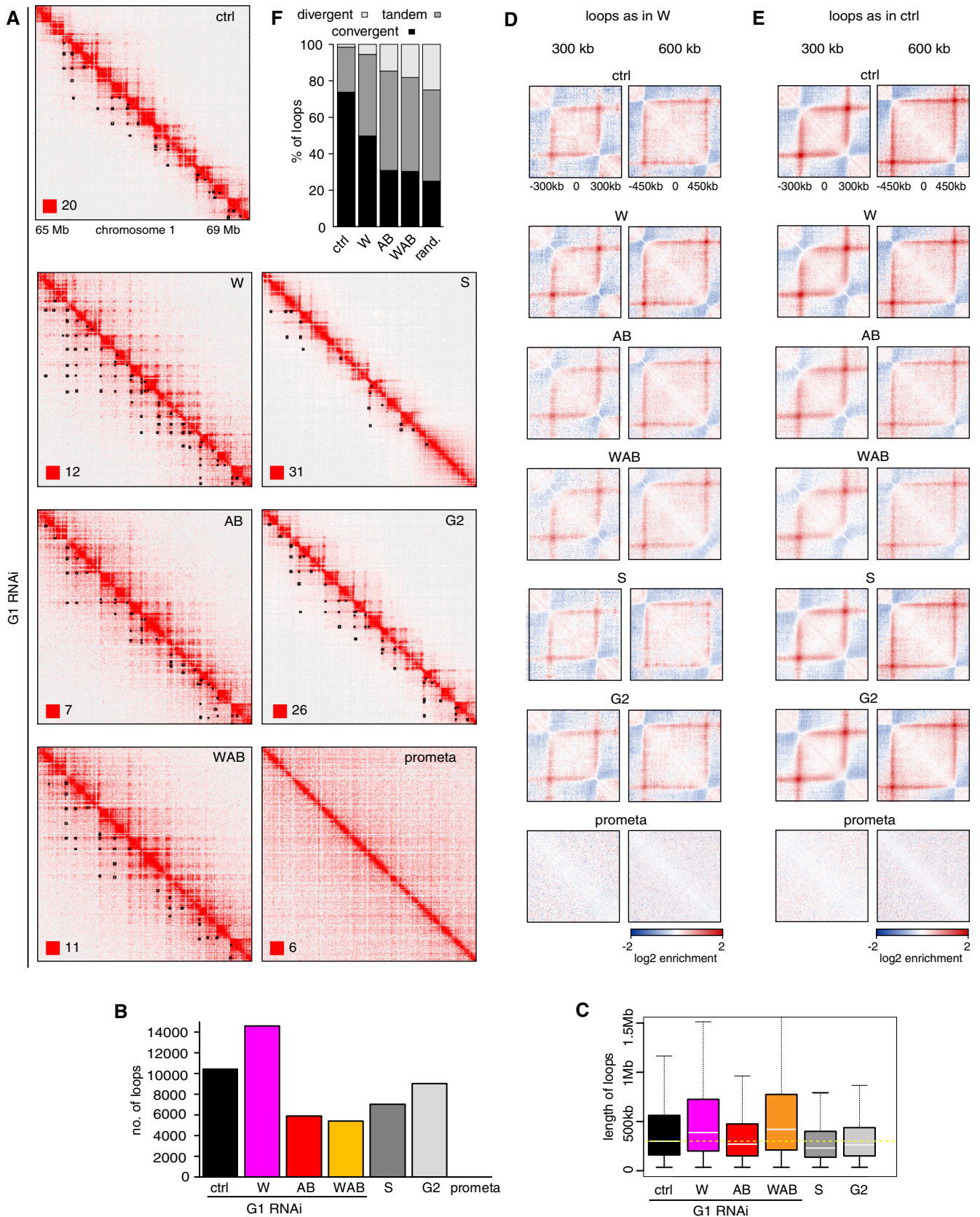


Figure 9.

Figure 9. WAPL and PDS5A/B RNAi depletion affect chromatin loops differently.

- A Coverage-corrected Hi-C contact matrices of the 65–69 Mb region of chromosome 1, for control-depleted (ctrl), WAPL-depleted (W), PDS5A/PDS5B-depleted (AB), and joint WAPL/PDS5A/PDS5B-depleted (WAB) cells in G1-phase, as well as S-phase (S), G2-phase (G2), and prometaphase (prometa) cells. Loops identified in this region are marked by black rectangles in the lower triangle. The matrices were plotted using Juicebox.
- B Number of loops in the same conditions as in (A). Colors are as in Fig 5C.
- C Loop length distribution in the same conditions as in (A). Colors are as in (B). Solid white lines mark the median, and boxes represent the middle 50% of the data. Whiskers denote all values of $1.5 \times$ interquartile range. Outliers are marked as dots and indicate values greater than $1.5 \times$ interquartile range. Yellow dotted line indicates the mean of the control.
- D Average contact enrichment around the 207×300 kb long and 82×600 kb long loops identified in WAPL-depleted cells but not in G1 control HeLa cells, for the same conditions.
- E Average contact enrichment around the 207×300 kb long and 82×600 kb long loops identified in G1 control HeLa cells, for the same conditions.
- F The proportion of convergent (black), tandem (dark gray), and divergent (light gray) CTCF binding orientation for loops with both anchors overlapping SMC3 and CTCF ChIP-seq peaks as well as unambiguous CTCF binding directions, for loops identified in control-depleted cells in G1-phase (ctrl, 2,691 loops), in WAPL-depleted but not in control-depleted cells in G1-phase (WAPL, 2,255 loops), in PDS5A/B-depleted but not in control-depleted cells in G1-phase (AB, 628 loops) and joint WAPL/PDS5A/PDS5B-depleted but not in control-depleted cells in G1-phase (WAB, 769 loops). The theoretically expected random proportions assuming no directionality bias are shown as comparison (rand.).

enabled by the increase in cohesin's residence time that WAPL depletion is known to cause (Tedeschi *et al*, 2013), which would allow cohesin to move along chromatin fibers with higher processivity (Fig EV5D). In addition, the increase in cohesin's copy number on chromatin that results from its increased residence time could also contribute to the frequency with which extended loops can be detected in WAPL-depleted cells, because it is possible that in control cells at steady state not all pairs of *loci* that could form loops are occupied by cohesin.

Interestingly, our analyses indicate that the shorter loops detected in control cells persist after WAPL depletion (Fig 9D). Conversely, the extended loops seen in WAPL-depleted cells can on average be detected in aggregate loop analyses in control cells (Fig 9E), even though these extended loops cannot be identified in these cells individually because they are below the detection limit. These observations imply that WAPL depletion does not lead to the formation of loops that cannot exist in control cells, but rather increases the frequency with which extended loops exist in the cell population.

WAPL is known to bind PDS5A and PDS5B (Kueng *et al*, 2006). Like WAPL, these proteins have been implicated in releasing cohesin from DNA (Rowland *et al*, 2009; Shintomi & Hirano, 2009; Ouyang *et al*, 2016), but PDS5 proteins also have positive functions in cohesion (for references, see Hons *et al*, 2016) and *in vitro* can promote loading of cohesin onto DNA (Murayama & Uhlmann, 2015). In agreement with a recent report (Ouyang *et al*, 2016), we found that depletion of PDS5 proteins can also increase cohesin's residence time on chromatin, although not to the same extent as depletion of WAPL, and cause chromatin compaction and cohesin accumulation in vermicelli. Despite these phenotypic similarities,

which are consistent with the idea that WAPL can release cohesin from DNA more efficiently in the presence of PDS5 proteins than in their absence, depletion of PDS5 proteins caused local changes in Hi-C interactions patterns that were strikingly different from those seen after WAPL depletion. Whereas WAPL depletion increased the number of detectable loops by 41.2%, co-depletion of PDS5A and PDS5B reduced loop numbers by 42.8% (Fig 9B). This effect of PDS5 depletion was dominant over the effect of WAPL depletion, as depletion of all three proteins reduced loop numbers by 49.0%. Despite these differences, depletion of WAPL and PDS5 proteins increased long-range interactions genome-wide in very similar ways (Fig 5C and D), resulting in the detectability of slightly fewer but larger TADs (Fig 7B and C), chromatin compaction, and vermicelli formation. These results imply that PDS5 proteins are not required for long-range chromatin interactions *per se*, but for their precise location. In other words, cells depleted of WAPL and PDS5 proteins may have similar numbers of loops, including extended loops, but in the former case, they might be formed more frequently between well-defined pairs of sequences, whereas in the latter, there may be more heterogeneity between loci that function as loop anchors, which would prevent their detection as specific corner peaks (i.e., loops) in Hi-C matrices. This particular phenotype caused by depletion of PDS5 proteins is similar to the effect of CTCF depletion, which also reduces the number of detectable loops (Fig 2K) without affecting the total number of long-range chromatin interactions genome-wide (Fig 2F). This phenotypic similarity raises the interesting possibility that the ability of CTCF to function as a boundary element in loop extrusion depends on PDS5 proteins (Fig EV5E).

How PDS5 proteins could perform this function is unclear, as is the mechanistic basis of CTCF's boundary function, but one

Figure 10. SCC1 degradation in WAPL and PDS5A/B RNAi depleted cells.

- A Analysis of the chromosome morphology changes after auxin addition in control-depleted and WAPL/PDS5A/B-depleted SCC1-mEGFP-AID cell lines that stably express mRaspberry-H2B by live-cell imaging. Scale bar indicates 5 μ m.
- B Chromatin volumetric changes in auxin-treated and untreated cells that have been depleted for control (left) and WAB (right). Chromatin volumes are normalized to the chromatin volumes at time 0 and plotted over time ($n > 7$ in each condition). Error bar depicts standard deviations of the means.
- C Coverage-corrected Hi-C contact matrices of chromosome 4, at 0 (left), 15 (center), and 180 min (right) after auxin addition to the WAPL/PDS5A/PDS5B-depleted SCC1-mEGFP-AID cell line. The matrices were plotted using Juicebox. The corresponding compartment signal tracks at 250 kb bin resolution are shown above the matrices.
- D Inter-chromosomal contact enrichment between bins with varying compartment signal strength from most B-like (1) to most A-like (50), for the same conditions as in (C).
- E Average contact enrichment around loops, for the 82×600 kb long loops identified in control-depleted G1 cells. The matrices are centered (0) around the halfway point of the loop anchor coordinates.
- F Coverage-corrected Hi-C contact matrices in the 88–94.5 Mb region of chromosome 12, for the same conditions as in (C). The matrices were plotted using Juicebox.

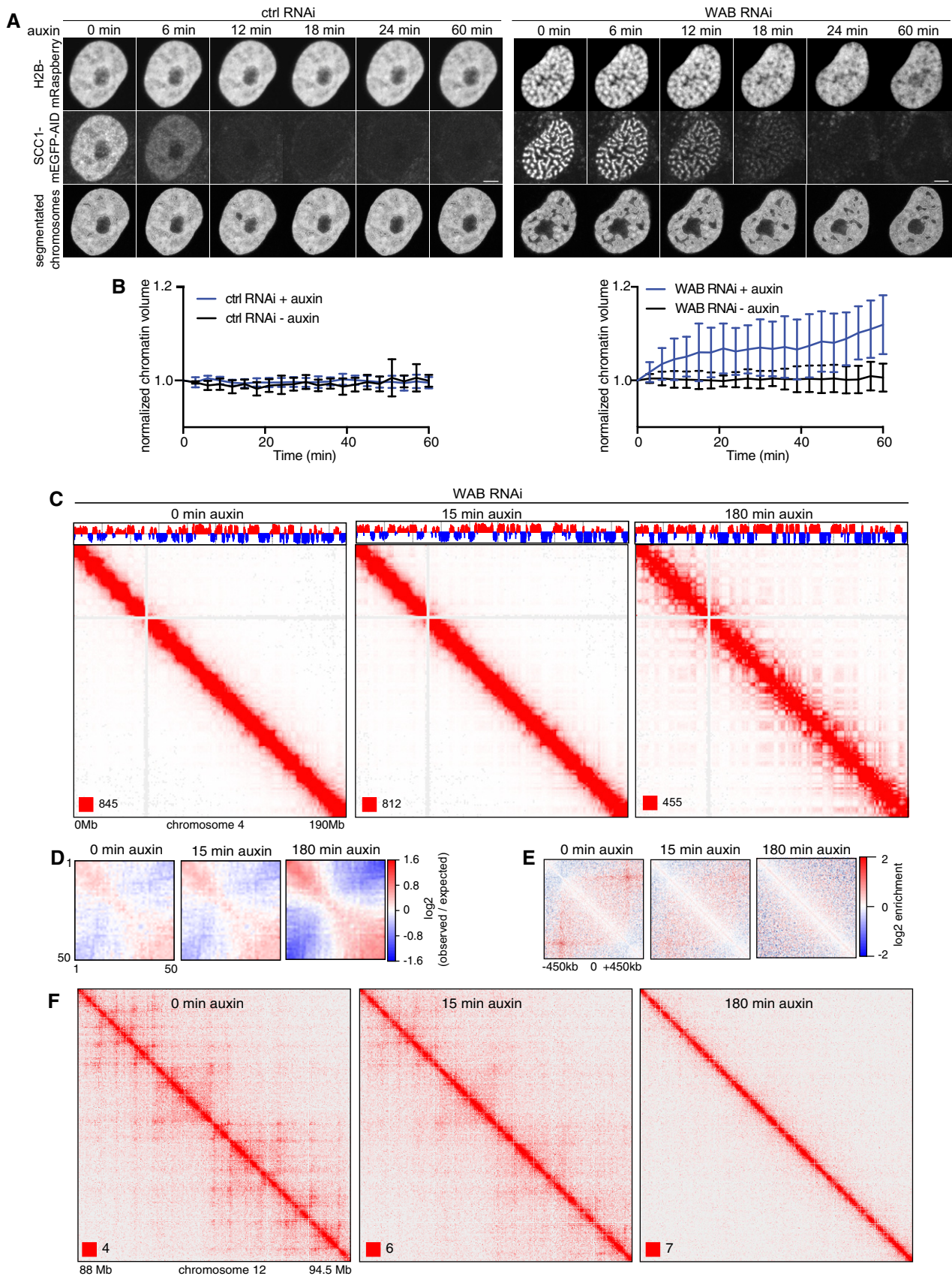


Figure 10.

possibility emerges from the previous observations that the cohesin loading complex stimulates cohesin's ATPase activity (Murayama & Uhlmann, 2013), is required for vermicelli formation (Haarhuis *et al*, 2017), and competes with PDS5 proteins for cohesin binding (Kikuchi *et al*, 2016). These findings would be consistent with the possibility that loop extrusion is mediated by cohesin's ATPase activity following its stimulation by the loading complex (as discussed by Rhodes *et al*, 2017), and that PDS5 proteins would inhibit this activity. If correct, our data imply that PDS5 proteins might mediate this effect in a CTCF-dependent manner. A different, but equally important question will be to understand how CTCF containing boundaries can be skipped to form extended loops. Our data show that this phenomenon occurs occasionally in wild-type cells but more frequently in cells depleted of WAPL and PDS5 proteins, that it leads to a violation of the CTCF convergence rule, and strongly suggest that, in cells depleted of WAPL and PDS5 proteins, it results in chromatin compaction and formation of vermicelli.

Materials and Methods

Generation of cell lines for auxin-mediated degradation

HeLa Kyoto cells were cultured as described previously (Nishiyama *et al*, 2010). The HeLa Kyoto cell line C-terminally tagged with a SCC1 AID was created by CRISPR/Cas9-mediated genome editing using a double-nickase strategy (Ran *et al*, 2013). The homologous recombination template used introduced the sequences coding for monomeric EGFP (L221K) and the *Arabidopsis thaliana* IAA1771-114 (AID*) mini-degron (Morawska & Ulrich, 2013). Single clones were selected by flow cytometry and confirmed to be homozygous by PCR. One of these clones was transduced with lentiviruses containing Tir1 from rice (*O. sativa*) using the plasmid pRRL-SOP (for SFFV, OsTir1, Puro), which comprises the constitutive promoter from spleen focus forming virus followed by OsTir1-3x-Myc-tag-T2A-Puro. The gRNAs sequences that were used for generating the SCC1 AID cell line were gRNA1: CACCGCAAATTGCCCCATGTGTA and gRNA2: CACCGCTTATATAATATGGAACCT. Primers used for genotyping were as follows: forward primer: TCAGGTATTGCC GCTGTTGT and reverse primer: GTGTGCAGCACTGAAAAGG. The CTCF-mEGFP-AID cell line was generated in the same way with gRNA sequences gRNA1: TCAGCATGATGGACCGGTGATGG, and gRNA2: TGAGGATCATCTCGGGCGTGAGG. The primers used for genotyping were as follows: forward primer: ACTGTTAATGTG GCGGGTT and reverse primer: CTGGGTGCCATTCTGCTACA.

Generation of homozygous mEGFP-tagged condensin cell lines

To endogenously tag the condensin I subunit CAP-D2 and the condensin II subunit CAP-D3 at the C-terminus with mEGFP in HeLa Kyoto cells, the paired CRISPR/Cas9 nickase approach was used as described in (Koch *et al*, 2017). After selecting GFP-positive cells by flow cytometry, single-cell clones were confirmed to be homozygously mEGFP-tagged at the endogenous locus by PCR, Southern blot and Western blot, respectively. For CAP-D2, only heterozygous clones were obtained after the first round of genome editing. Since Sanger sequencing revealed the untagged alleles not to be mutated,

a second round of genome editing was performed like the first round and resulted in a homozygously tagged clone. Correct subcellular localization of homozygously mEGFP-tagged proteins during the cell cycle was confirmed by confocal microscopy. Furthermore, the mitotic timing was shown to be unperturbed using automated time-lapse wide-field microscopy and automatic classification of cells into interphase and mitotic stages. Finally, GFP immunoprecipitation and immunoblotting against all subunits of the condensin complex showed that the formation of pentameric condensin complexes was not prevented by the introduced tag in both asynchronous and nocodazole-arrested mitotic cell populations. The details of all cell line validation steps are described in Koch *et al* (2017).

Synchronization protocol

Cells were synchronized at the G1/S-phase boundary by two consecutive arrest phases with 2 mM thymidine and released into fresh medium for 2 h (S-phase), 6 h (G2-phase), or 15 h (G1-phase). For prometaphase arrest, cells were released from double-thymidine block and 8 h later Nocodazole was added at a concentration of 100 ng/ml. Five hours later, PM cells were removed by shake off. For each cell cycle stage, cells were fixed for Hi-C, microscopy, and FACS, respectively. Cell cycle profiling was performed using propidium iodide staining (Ladurner *et al*, 2014).

RNA interference

For RNAi experiments, the cells were transfected with siRNAs as described previously (van der Lelij *et al*, 2014) just before adding thymidine. The following target sequences of siRNAs (Ambion) were used: WAPL (5'-CGGACUACCCUUAGCACAAtt-3'), PDS5A (5'-GCUCCAUAUACUCCCAUGtt-3'), PDS5B (5'-GAGACGACUCUGAUCUUGUtt-3'), NIPBL (5'-GCAUCGGUAUCAAGUCCCAAtt-3') and SMC2 (5'-UGCUAUCACUGGCUUAAAUtt-3'). The cells were transfected by incubating duplex siRNA with RNAi-MAX transfection reagent in antibiotic-free growth medium at 100 nM. After 72 h of RNAi treatment, cells were harvested for the experiments.

Chromatin fractionation

Cells were extracted in a buffer consisting of 20 mM Tris-HCl (pH 7.5), 100 mM NaCl, 5 mM MgCl₂, 2 mM NaF, 10% glycerol, 0.2% NP40, 20 mM β-glycerophosphate, 0.5 mM DTT, and protease inhibitor cocktail (Complete EDTA-free, Roche). Chromatin pellets and supernatant were separated and collected by centrifugation at 2,000 g for 5 min. The chromatin pellets were washed three times with the same buffer.

Antibodies

NIPBL antibodies were a generous gift from Tom Strachan (Seitan *et al*, 2006). MAU2 antibodies were reported previously (Watrin *et al*, 2006). Rabbit anti-CTCF (Peters laboratory A992) was reported previously (Busslinger *et al*, 2017). The following commercial antibodies were used: SMC1 (Bethyl Laboratories, A300-055A), SMC3 (Bethyl Laboratories, A300-060A), SCC1 (EMD Millipore Corporation, 53A303), PDS5A (Bethyl Laboratories, A300-089A),

α -tubulin (Sigma-Aldrich, T5168), histone H3 (Santa Cruz Biotechnology, sc-8654), phospho-histone H3 (Ser10) (Cell Signaling, 9701), GFP (Roche, clones 7.1 and 13.1; Abcam, ab13970), aurora B (BD Transduction Laboratory, 611083). The following secondary antibodies were used: goat anti-rabbit IgG Alexa-Fluor-488 and -568, anti-mouse IgG Alexa-Fluor-488, -568 (Molecular Probes) for IF and anti-rabbit or mouse Ig, HRP-linked whole antibody (GE Healthcare) and polyclonal rabbit anti-goat or anti-rat immunoglobulins/HRP (Dako) for WB.

Immunofluorescence

Cells were fixed with 4% formaldehyde for 10 min at room temperature and permeabilized with 0.2% Triton X-100 in PBS for 5 min. Pre-extraction was carried out for 1 min in 0.1% Triton X-100 in PBS before fixation. After blocking in 3% BSA in PBS-T 0.01% for 1 h, the cells were incubated with the primary antibodies overnight at 4°C and subsequently incubated with the secondary antibodies for 1 h at room temperature. After counterstaining the DNA by 10 min incubation in 0.1 μ M DAPI in PBS, the chambers were perfused with vector shield (Vector Laboratories) before imaging.

Live-cell imaging

SCC1-mEGFP-AID cells were seeded on Lab-Tek chambered coverslips (Thermo Scientific Nunc) and treated with control or WAPL, PDS5A, and PDS5B siRNAs for 72 h. Before imaging, the culture medium was exchanged for pre-warmed CO₂-independent medium (Gibco). DNA was visualized by staining with 0.5 μ M SiR-DNA (Spirochrome, CHF280.00) or stably expressing mRaspberry-H2B. Imaging was performed with a LSM780 confocal microscope (Carl Zeiss), using a 63 \times /1.4 numerical aperture (N/A) objective. After treatment with 500 μ M auxin, three-dimensional images with 520 \times 520 \times 35 voxels (voxel size $x \times y \times z$: 100 \times 100 \times 500 nm) were collected every 3 min, or two-dimensional images with 1,568 \times 1,568 pixels (pixel size $x \times y$: 108 \times 108 nm) every 2 min.

Inverse fluorescence recovery after photobleaching (iFRAP)

SCC1-mEGFP cells that stably express DHB-mKate2 and that had been depleted for control, W, AB, or WAB were imaged on a LSM780 confocal microscope (Carl Zeiss), using a 63 \times /1.4 numerical aperture (N/A) objective. Two images were acquired before bleaching half of the nucleus by 100% transmission of a 488 nm laser. The recovery was quantified using the ZEN2011 software, as the difference between the mean fluorescence signal intensity of the bleached and the unbleached regions. G1-phase cells were identified by nuclear localization of DHB-mKate2 signals (Spencer *et al*, 2013).

ChIP-seq peak calling and calculation of peak overlaps

Cohesin (SMC3) and CTCF ChIP were performed as described in Wendt *et al* (2008). Peaks were called by the MACS algorithm version 1.4.2 (Zhang *et al*, 2008), using a *P*-value threshold of 1e-10 and by using sample and input read files. We identified sites of overlapping peaks between different conditions as well as between SMC3 and CTCF peaks using the MULTOVL software (Aszodi, 2012). We applied an inclusive type of overlap display (“union”), in

which coordinates of overlapping peaks are merged into one common genomic site.

Hi-C library preparation

Hi-C libraries were generated as described in Nagano *et al* (2015), with modifications as described below. 3 to 4 \times 10⁷ HeLa cells were fixed in 2% formaldehyde (Agar Scientific) for 10 min, after which the reaction was quenched with ice-cold glycine (Sigma; 0.125 M final concentration). Cells were collected by centrifugation (400 \times *g* for 10 min at 4°C) and washed once with 50 ml PBS pH 7.4 (Gibco). After another centrifugation step (400 \times *g* for 10 min at 4°C), the supernatant was completely removed and the cell pellets were immediately frozen in liquid nitrogen and stored at -80°C. After thawing, the cell pellets were incubated in 50 ml ice-cold lysis buffer [10 mM Tris-HCl pH 8, 10 mM NaCl, 0.2% Igepal CA-630, protease inhibitor cocktail (Roche)] for 30 min on ice. After centrifugation to pellet the cell nuclei (650 \times *g* for 5 min at 4°C), nuclei were washed once with 1.25 \times NEBuffer 2 (NEB). The nuclei were then resuspended in 1.25 \times NEBuffer 2, SDS (10% stock; Promega) was added (0.3% final concentration), and the nuclei were incubated at 37°C for 1 h with agitation (950 rpm). Triton X-100 (Sigma) was added to a final concentration of 1.7%, and the nuclei were incubated at 37°C for 1 h with agitation (950 rpm). Restriction digest was performed overnight at 37°C with agitation (950 rpm) with *HindIII* (NEB; 1,500 units per 7 million cells). Using biotin-14-dATP (Life Technologies), dCTP, dGTP, and dTTP (Life Technologies; all at a final concentration of 30 μ M), the *HindIII* restriction sites were then filled in with Klenow (NEB) for 75 min at 37°C. The ligation was performed for 4 h at 16°C (50 units T4 DNA ligase (Life Technologies) per 7 million cells starting material) in a total volume of 5.5 ml ligation buffer (50 mM Tris-HCl, 10 mM MgCl₂, 1 mM ATP, 10 mM DTT, 100 μ g/ml BSA, 0.9% Triton X-100) per 7 million cells starting material. After ligation, crosslinking was reversed by incubation with proteinase K (Roche; 65 μ l of 10 mg/ml per 7 million cells starting material) at 65°C overnight. An additional proteinase K incubation (65 μ l of 10 mg/ml per 7 million cells starting material) at 65°C for 2 h was followed by RNase A (Roche; 15 μ l of 10 mg/ml per 7 million cells starting material) treatment and two sequential phenol/chloroform (Sigma) extractions. After DNA precipitation [sodium acetate 3 M pH 5.2 (1/10 volume) and ethanol (2.5 \times volumes)] overnight at -20°C, the DNA was spun down (centrifugation 3,200 \times *g* for 30 min at 4°C). The pellets were resuspended in 400 μ l TLE (10 mM Tris-HCl pH 8.0; 0.1 mM EDTA) and transferred to 1.5-ml Eppendorf tubes. After another phenol/chloroform (Sigma) extraction and DNA precipitation overnight at -20°C, the pellets were washed three times with 70% ethanol, and the DNA concentration was determined using Quant-iT Pico Green (Life Technologies).

To remove biotin from non-ligated fragment ends, 30–40 μ g of Hi-C library DNA was incubated with T4 DNA polymerase (NEB) for 4 h at 20°C, followed by phenol/chloroform purification and DNA precipitation overnight at -20°C. After a wash with 70% ethanol, sonication was carried out to generate DNA fragments with a size peak around 400 bp (Covaris E220 settings: duty factor: 10%; peak incident power: 140 W; cycles per burst: 200; time: 55 s). After end repair [T4 DNA polymerase, T4 DNA polynucleotide kinase, Klenow (all NEB) in the presence of dNTPs in

ligation buffer (NEB)] for 30 min at room temperature, the DNA was purified (Qiagen PCR purification kit). dATP was added with Klenow exo- (NEB) for 30 min at 37°C, after which the enzyme was heat-inactivated (20 min at 65°C). A double-size selection using AMPure XP beads (Beckman Coulter) was performed: First, the ratio of AMPure XP beads solution volume to DNA sample volume was adjusted to 0.6:1. After incubation for 15 min at room temperature, the sample was transferred to a magnetic separator (DynaMag-2 magnet; Life Technologies), and the supernatant was transferred to a new Eppendorf tube, while the beads were discarded. The ratio of AMPure XP beads solution volume to DNA sample volume was then adjusted to 0.9:1 final. After incubation for 15 min at room temperature, the sample was transferred to a magnet (DynaMag-2 magnet; Life Technologies). Following two washes with 70% ethanol, the DNA was eluted in 100 µl of TLE (10 mM Tris-HCl pH 8.0; 0.1 mM EDTA). Biotinylated ligation products were isolated using MyOne Streptavidin C1 Dynabeads (Life Technologies) on a DynaMag-2 magnet (Life Technologies) in binding buffer (5 mM Tris pH8, 0.5 mM EDTA, 1 M NaCl) for 30 min at room temperature. After two washes in binding buffer and one wash in ligation buffer (NEB), PE adapters (Illumina) were ligated onto Hi-C ligation products bound to streptavidin beads for 2 h at room temperature (T4 DNA ligase NEB, in ligation buffer, slowly rotating). After washing twice with wash buffer (5 mM Tris, 0.5 mM EDTA, 1 M NaCl, 0.05% Tween-20) and then once with binding buffer, the DNA-bound beads were resuspended in a final volume of 90 µl NEBuffer 2. Bead-bound Hi-C DNA was amplified with 7 PCR amplification cycles (36–40 individual PCRs) using PE PCR 1.0 and PE PCR 2.0 primers (Illumina). After PCR amplification, the Hi-C libraries were purified with AMPure XP beads (Beckman Coulter). The concentration of the Hi-C libraries was determined by Bioanalyzer profiles (Agilent Technologies) and qPCR (Kapa Biosystems), and the Hi-C libraries were paired-end sequenced (HiSeq 1000, Illumina) at the Babraham Institute Sequencing Facility and (HiSeqv4, Illumina) at VBCF NGS.

Hi-C analyses

Hi-C data processing and normalization

Raw sequencing reads were processed using the HiCUP pipeline (Wingett et al, 2015). Positions of di-tags were mapped against the human genome (hg19), and experimental artifacts, such as circularized reads and re-ligations, were filtered out, and duplicate reads were removed. Library statistics are presented in Table EV1. Aligned Hi-C data were normalized using HOMER v4.7 (Heinz et al, 2010) and Juicer tools v0.7.5 (Durand et al, 2016). Using binned Hi-C data, we computed the coverage- and distance-related background in the Hi-C data employing matrix balancing algorithms at 25 kb, 250 kb, 1 Mb (iterative correction by HOMER) and 2.5 Mb, 1 Mb, 500 kb, 250 kb, 100 kb, 50 kb, 25 kb, 10 kb, and 5 kb (Knight–Ruiz balancing by Juicer tools) resolutions. General genome organization in the eight selected conditions was compared by plotting the coverage-corrected and the distance-and-coverage-corrected Hi-C matrices.

Intra-chromosomal contact frequency analysis

We plotted the frequency of cis-chromosomal contacts in the raw data at various genomic distances. The frequency density was

obtained by binning all cis-chromosomal contact distances (or, alternatively, the log₁₀ distances), using 100 bins of equal size on a log₁₀ genomic distance plot between 0 (1 bp) and 10 (10 Gb).

Compartment analysis

The compartment signal was computed as the first principle component of the distance-and-coverage-corrected interaction profile correlation matrix (Lieberman-Aiden et al, 2009) at 250 kb resolution, with positive values aligned with H3K4me3 ChIP-seq on HeLa cells (<https://www.encodeproject.org/experiments/ENCSTR000DUA/>; <https://www.encodeproject.org/experiments/ENCFF001XCR/>). For chromosomes for which the contact enrichment within chromosome arms was stronger than the compartment signal, we used the second principal component. The compartment signal for the selected conditions in each replicate was plotted for comparison, and the genome-wide concatenated ChIP-seq aligned principal components were clustered using hierarchical clustering (using 1—Pearson correlation as the distance metric).

Using all A- and B-compartment bins defined by positive and negative compartment signal values in the control dataset, we also defined a compartmentalization score, measuring the $-\log_2$ enrichment of trans-chromosomal contacts between all A- and B-compartment bins:

Compartment score = $-\log_2 (2 P(A) P(B) T/O_{AB})$ where $T = O_{AA} + O_{AB} + O_{BB}$ and $P(A) = (2O_{AA} + O_{AB})/2T$, where O_{AA} , O_{AB} , and O_{BB} are the number of observed trans-chromosomal or long-cis (> 2 Mb) chromosomal contacts between all A–A, A–B, and B–B bin pairs.

We defined 50 compartment groups of increasing A-compartment association, by binning all 250 kb bins of the genome into 50 equally sized groups according to their compartment signal in the G1-rep1 dataset. Group 1 contains 250 kb bins with most negative compartment signal values (strongly B-compartment like) and group 50 contains 250 kb bins with most positive compartment signal values (strongly A-compartment like). To obtain a pairwise contact enrichment matrix between these 50 groups, we computed the log₂ enrichment of contacts between any two groups over the contact counts using a +10 Mb shifted compartment signal of the G1-rep1 dataset, with a correction to match the coverage profile of the 50 groups in the observed data.

Data availability

The Hi-C and ChIP-seq sequencing data from this publication have been deposited in the Gene Expression Omnibus (GEO) under the accession number GSE102884.

Expanded View for this article is available online.

Acknowledgements

We are grateful to Marina M Kavur for providing the Mad2L-EGFP cell line and Georg Busslinger for MEFs. We thank Iain F Davidson and Benedikt Bauer for helpful discussions, Kristina Tabbada and VBCF for next-generation sequencing, and Steven W. Wingett for Hi-C data mapping. Research in the laboratory of JMP is supported by Boehringer Ingelheim, the Austrian Science Fund (FWF special research program SFB F34 “Chromosome Dynamics” and Wittgenstein award Z196-B20), and the Austrian Research Promotion Agency (Headquarter grants FFG-834223). SS and PF are supported by the UK Biotechnology and

Biological Sciences Research Council (BB/J004480/1) and CV and PF by the European Research Council Advanced Grant (DEVOCHROMO). KN is supported by an EMBO Long Term Fellowship (ALTF 1335-2016) and a HFSP fellowship (LT001527/2017). DAC acknowledges the VIPS Program of the Austrian Federal Ministry of Science and Research and the City of Vienna. JE acknowledges funding from the 4D Nucleome/4DN NIH Common Fund (U01 EB021223), by the European Molecular Biology Laboratory (JE, MJH) and the EMBL International PhD Programme (NW).[†]

Author contributions

GW, KN, DAC, and J-MP designed experiments and interpreted data together with CV, RRS, and SS. Cell lines were generated by MM and DAC (SCC1-mEGFP-AID with and without H2B-mCherry), WT (CTCF-mEGFP-AID), and NW, BK, MK (CAP-D2-mEGFP, CAP-D3-mEGFP). KN, DAC, and GW performed RNAi, immunoblotting and microscopy experiments. GJ quantified chromatin compaction phenotypes. WT performed ChIP-seq experiments. MJH developed an algorithm for chromatin volume analysis. GW generated the Hi-C libraries with help from SS. CV and RRS performed bioinformatic analyses of Hi-C data with input from GW. RRS analyzed ChIP-seq data. JE, JZ, PF, and J-MP supervised the project. GW, CV, KN, DAC, and J-MP wrote the manuscript.

Conflict of interest

The authors declare that they have no conflict of interest.

References

- Alipour E, Marko JF (2012) Self-organization of domain structures by DNA-loop-extruding enzymes. *Nucleic Acids Res* 40: 11202–11212
- Aszodi A (2012) MULTOVL: fast multiple overlaps of genomic regions. *Bioinformatics* 28: 3318–3319
- Bell AC, Felsenfeld G (2000) 1–30 Methylation of a CTCF-dependent boundary controls imprinted expression of the *Igf2* gene. *Nature* 405: 482–485
- Blat Y, Protacio RU, Hunter N, Kleckner N (2002) Physical and functional interactions among basic chromosome organizational features govern early steps of meiotic chiasma formation. *Cell* 111: 791–802
- Busslinger GA, Stocsits RR, van der Lelij P, Axelsson E, Tedeschi A, Galjart N, Peters J-M (2017) Cohesin is positioned in mammalian genomes by transcription, CTCF and Wapl. *Nature* 544: 503–507
- Chan KL, Roig MB, Hu B, Beckouët F, Metson J, Nasmyth K (2012) Cohesin's DNA exit gate is distinct from its entrance gate and is regulated by acetylation. *Cell* 150: 961–974
- Davidson IF, Goetz D, Zaczek MP, Molodtsov MI, Huis in 't Veld PJ, Weissmann F, Litos G, Cisneros DA, Ocampo-Hafalla M, Ladurner R, Uhlmann F, Vaziri A, Peters J (2016) Rapid movement and transcriptional re-localization of human cohesin on DNA. *EMBO J* 35: e201695402
- Dewar H, Tanaka K, Nasmyth K, Tanaka TU (2004) Tension between two kinetochores suffices for their bi-orientation on the mitotic spindle. *Nature* 428: 93–97
- Dixon JR, Selvaraj S, Yue F, Kim A, Li Y, Shen Y, Hu M, Liu JS, Ren B (2012) Topological domains in mammalian genomes identified by analysis of chromatin interactions. *Nature* 485: 376–380
- Dorsett D, Merkenschlager M (2013) Cohesin at active genes: a unifying theme for cohesin and gene expression from model organisms to humans. *Curr Opin Cell Biol* 25: 327–333
- Durand NC, Shamim MS, Machol I, Rao SSP, Huntley MH, Lander ES, Aiden EL (2016) Juicer provides a one-click system for analyzing loop-resolution Hi-C experiments. *Cell Syst* 3: 95–98
- Earnshaw WC, Laemmli UK (1983) Architecture of metaphase chromosomes and chromosome scaffolds. *J Cell Biol* 96: 84–93
- Flyamer IM, Gassler J, Imakaev M, Brandão HB, Ulianov SV, Abdennur N, Razin SV, Mirny LA, Tachibana-Konwalski K (2017) Single-nucleus Hi-C reveals unique chromatin reorganization at oocyte-to-zygote transition. *Nature* 544: 110–114
- Fudenberg G, Imakaev M, Lu C, Goloborodko A, Abdennur N, Mirny LA (2016) Formation of chromosomal domains by loop extrusion. *Cell Rep* 15: 2038–2049
- Gandhi R, Gillespie PJ, Hirano T (2006) Human WAPL is a cohesin-binding protein that promotes sister-chromatid resolution in mitotic prophase. *Curr Biol* 16: 2406–2417
- Gassler J, Brandão HB, Imakaev M, Flyamer IM, Ladstätter S, Bickmore WA, Peters JM, Mirny LA, Tachibana K (2017) A mechanism of cohesin-dependent loop extrusion organizes zygotic genome architecture. *EMBO J* 36: 3600–3618
- Gerlich D, Koch B, Dupeux F, Peters JM, Ellenberg J (2006) Live-cell imaging reveals a stable cohesin-chromatin interaction after but not before DNA replication. *Curr Biol* 16: 1571–1578
- Gruber S (2014) Multilayer chromosome organization through DNA bending, bridging and extrusion. *Curr Opin Microbiol* 22: 102–110
- Guacci V, Koshland D, Strunnikov A (1997) A direct link between sister chromatid cohesion and chromosome condensation revealed through the analysis of MCD1 in *S. cerevisiae*. *Cell* 91: 47–57
- Haarhuis JHI, van der Weide RH, Blomen VA, Yáñez-Cuna JO, Amendola M, van Ruiten MS, Krijger PHL, Teunissen H, Medema RH, van Steensel B, Brummelkamp TR, de Wit E, Rowland BD (2017) The cohesin release factor WAPL restricts chromatin loop extension. *Cell* 169: 693–707.e14
- Hadjur S, Williams LM, Ryan NK, Cobb BS, Sexton T, Fraser P, Fisher AG, Merkenschlager M (2009) Cohesins form chromosomal cis-interactions at the developmentally regulated *IFNG* locus. *Nature* 460: 410–413
- Haering CH, Farcas A-M, Arumugam P, Metson J, Nasmyth K (2008) The cohesin ring concatenates sister DNA molecules. *Nature* 454: 297–301
- Hark AT, Schoenherr CJ, Katz DJ, Ingram RS, Levorse JM, Tilghman SM (2000) CTCF mediates methylation-sensitive enhancer-blocking activity at the *H19/Igf2* locus. *Nature* 405: 486–489
- Heidinger-Pauli JM, Mert O, Davenport C, Guacci V, Koshland D (2010) Systematic reduction of cohesin differentially affects chromosome segregation, condensation, and DNA repair. *Curr Biol* 20: 957–963
- Heinz S, Benner C, Spann N, Bertolino E, Lin YC, Laslo P, Cheng JX, Murre C, Singh H, Glass CK (2010) Simple combinations of lineage-determining transcription factors prime cis-regulatory elements required for macrophage and B cell identities. *Mol Cell* 38: 576–589
- Hons MT, Huis in 't Veld PJ, Kaesler J, Rombaut P, Schleiffer A, Herzog F, Stark H, Peters J-M (2016) Topology and structure of an engineered human cohesin complex bound to Pds5B. *Nat Commun* 7: 12523
- Huis in 't Veld PJ, Herzog F, Ladurner R, Davidson IF, Piric S, Kreidl E, Bhaskara V, Aebersold R, Peters J-M (2014) Characterization of a DNA exit gate in the human cohesin ring. *Science* 346: 968–972

[†]Correction added on 15 December 2017, after first online publication: the Acknowledgements have been updated.

- Kagey MH, Newman JJ, Bilodeau S, Zhan Y, Orlando DA, van Berkum NL, Ebmeier CC, Goossens J, Rahl PB, Levine SS, Taatjes DJ, Dekker J, Young RA (2010) Mediator and cohesin connect gene expression and chromatin architecture. *Nature* 467: 430–435
- Kanke M, Tahara E, Huis in 't Veld PJ, Nishiyama T (2016) Cohesin acetylation and Wapl-Pds5 oppositely regulate translocation of cohesin along DNA. *EMBO J* 35: 2686–2698
- Kikuchi S, Borek DM, Otwinowski Z, Tomchick DR, Yu H (2016) Crystal structure of the cohesin loader Scc2 and insight into cohesinopathy. *Proc Natl Acad Sci* 113: 12444–12449
- Klein F, Mahr P, Galova M, Buonomo SBC, Michaelis C, Nairz K, Nasmyth K (1999) A central role for cohesins in sister chromatid cohesion, formation of axial elements, and recombination during yeast meiosis. *Cell* 98: 91–103
- Koch B, Nijmeijer B, Kueblbeck M, Cai Y, Walther N, Ellenberg J (2017) Generation and validation of homozygous fluorescent knock-in cells using genome editing. *bioRxiv* <https://doi.org/10.1101/173633> [PREPRINT]
- Kubo N, Ishii H, Gorkin D, Meitinger F, Xiong X, Fang R, Liu T, Ye Z, Li B, Dixon J, Desai A, Zhao H, Ren B (2017) Preservation of chromatin organization after acute loss of CTCF in mouse embryonic stem cells. *bioRxiv* <https://doi.org/10.1101/118737> [PREPRINT]
- Kueng S, Hegemann B, Peters BH, Lipp JJ, Schleiffer A, Mechtler K, Peters JM (2006) Wapl Controls the Dynamic Association of Cohesin with Chromatin. *Cell* 127: 955–967
- Kurukuti S, Tiwari VK, Tavoosidana G, Pugacheva E, Murrell A, Zhao Z, Lobanenko V, Reik W, Ohlsson R (2006) CTCF binding at the H19 imprinting control region mediates maternally inherited higher-order chromatin conformation to restrict enhancer access to Igf2. *Proc Natl Acad Sci USA* 103: 10684–10689
- Ladurner R, Bhaskara V, Huis in 't Veld PJ, Davidson IF, Kreidl E, Petzold G, Peters JM (2014) Cohesin's ATPase activity couples cohesin loading onto DNA with Smc3 acetylation. *Curr Biol* 24: 2228–2237
- Lajoie BR, Dekker J, Kaplan N (2015) The Hitchhiker 's guide to Hi-C analysis : practical guidelines. *Methods* 72: 65–75
- van der Lelij P, Stocsits RR, Ladurner R, Petzold G, Kreidl E, Koch B, Schmitz J, Neumann B, Ellenberg J, Peters J-M (2014) SNW1 enables sister chromatid cohesion by mediating the splicing of sororin and APC2 pre-mRNAs. *EMBO J* 33: 2643–2658
- Lengronne A, Pasero P (2014) Closing the MCM cycle at replication termination sites. *EMBO Rep* 15: e201439774
- Lieberman-Aiden E, van Berkum NL, Williams L, Imakaev M, Ragoczy T, Telling A, Amit I, Lajoie BR, Sabo PJ, Dorschner MO, Sandstrom R, Bernstein B, Bender MA, Groudine M, Gnirke A, Stamatoyannopoulos J, Mirny LA, Lander ES, Dekker J (2009) Comprehensive mapping of long-range interactions reveals folding principles of the human genome. *Science* 326: 289–293
- Losada A, Hirano M, Hirano T (1998) Identification of *Xenopus* SMC protein complexes required for sister chromatid cohesion. *Genes Dev* 12: 1986–1997
- Michaelis C, Ciosk R, Nasmyth K (1997) Cohesins: chromosomal proteins that prevent premature separation of sister chromatids. *Cell* 91: 35–45
- Mishiro T, Ishihara K, Hino S, Tsutsumi S, Aburatani H, Shirahige K, Kinoshita Y, Nakao M (2009) Architectural roles of multiple chromatin insulators at the human apolipoprotein gene cluster. *EMBO J* 28: 1234–1245
- Morawska M, Ulrich HD (2013) An expanded tool kit for the auxin-inducible degron system in budding yeast. *Yeast* 30: 341–351
- Murayama Y, Uhlmann F (2013) Biochemical reconstitution of topological DNA binding by the cohesin ring. *Nature* 505: 367–371
- Murayama Y, Uhlmann F (2015) DNA entry into and exit out of the cohesin ring by an interlocking gate mechanism. *Cell* 163: 1628–1640
- Nagano T, Várnai C, Schoenfelder S, Javierre B-M, Wingett SW, Fraser P (2015) Comparison of Hi-C results using in-solution versus in-nucleus ligation. *Genome Biol* 16: 175
- Nagano T, Lubling Y, Várnai C, Dudley C, Leung W, Baran Y, Mendelson Cohen N, Wingett S, Fraser P, Tanay A (2017) Cell-cycle dynamics of chromosomal organization at single-cell resolution. *Nature* 547: 61–67
- Narendra V, Rocha PP, An D, Raviram R, Skok JA, Mazzoni EO, Reinberg D (2015) Transcription. CTCF establishes discrete functional chromatin domains at the Hox clusters during differentiation. *Science* 347: 1017–1021
- Nasmyth K (2001) Disseminating the genome: joining, resolving, and separating sister chromatids during mitosis and meiosis. *Annu Rev Genet* 35: 673–745
- Nativio R, Wendt KS, Ito Y, Huddleston JE, Uribe-Lewis S, Woodfine K, Krueger C, Reik W, Peters JM, Murrell A (2009) Cohesin is required for higher-order chromatin conformation at the imprinted IGF2-H19 locus. *PLoS Genet* 5: e1000739
- Naumova N, Imakaev M, Fudenberg G, Zhan Y, Lajoie BR, Mirny LA, Dekker J (2013) Organization of the mitotic chromosome. *Science* 342: 948–953
- Nishimura K, Fukagawa T, Takisawa H, Kakimoto T, Kanemaki M (2009) An auxin-based degron system for the rapid depletion of proteins in nonplant cells. *Nat Methods* 6: 917–922
- Nishiyama T, Ladurner R, Schmitz J, Kreidl E, Schleiffer A, Bhaskara V, Bando M, Shirahige K, Hyman AA, Mechtler K, Peters JM (2010) Sororin mediates sister chromatid cohesion by antagonizing Wapl. *Cell* 143: 737–749
- Nora EP, Lajoie BR, Schulz EG, Giorgetti L, Okamoto I, Servant N, Piolot T, van Berkum NL, Meisig J, Sedat J, Gribnau J, Barillot E, Blüthgen N, Dekker J, Heard E (2012) Spatial partitioning of the regulatory landscape of the X-inactivation centre. *Nature* 485: 381–385
- Nora EP, Goloborodko A, Valton AL, Gibcus JH, Uebersohn A, Abdennur N, Dekker J, Mirny LA, Bruneau BG (2017) Targeted degradation of CTCF decouples local insulation of chromosome domains from genomic compartmentalization. *Cell* 169: 930–944.e22
- Ono T, Losada A, Hirano M, Myers MP, Neuwald AF, Hirano T (2003) Differential contributions of condensin I and condensin II to mitotic chromosome architecture in vertebrate cells. *Cell* 115: 109–121
- Ouyang Z, Zheng G, Tomchick DR, Luo X, Yu H (2016) Structural basis and IP6 requirement for Pds5-dependent cohesin dynamics. *Mol Cell* 62: 248–259
- Parelho V, Hadjur S, Spivakov M, Leleu M, Sauer S, Gregson HC, Jarmuz A, Canzonetta C, Webster Z, Nesterova T, Cobb BS, Yokomori K, Dillon N, Aragon L, Fisher AG, Merkenschlager M (2008) Cohesins functionally associate with CTCF on mammalian chromosome arms. *Cell* 132: 422–433
- Pauli A, Althoff F, Oliveira RA, Heidmann S, Schuldiner O, Lehner CF, Dickson BJ, Nasmyth K (2008) Cell-type-specific TEV protease cleavage reveals cohesin functions in *Drosophila* neurons. *Dev Cell* 14: 239–251
- Peters JM, Tedeschi A, Schmitz J (2008) The cohesin complex and its roles in chromosome biology. *Genes Dev* 22: 3089–3114
- Ran FA, Hsu PD, Lin CY, Gootenberg JS, Konermann S, Trevino AE, Scott DA, Inoue A, Matoba S, Zhang Y, Zhang F (2013) Double nicking by RNA-guided CRISPR cas9 for enhanced genome editing specificity. *Cell* 154: 1380–1389
- Rao SSP, Huntley MH, Durand NC, Stamenova EK, Bochkov ID, Robinson JT, Sanborn AL, Machol I, Omer AD, Lander ES, Aiden EL (2014) A 3D map of

- the human genome at kilobase resolution reveals principles of chromatin looping. *Cell* 159: 1665–1680
- Rao SSP, Huang S-C, Hilaire BGS, Engreitz JM, Perez EM, Kieffer-Kwon K-R, Sanborn AL, Johnstone SE, Bascom GD, Bochkov ID, Huang X, Shamim MS, Shin J, Turner D, Ye Z, Omer AD, Robinson JT, Schlick T, Bernstein BE, Casellas R et al (2017) Cohesin loss eliminates all loop domains. *Cell* 171: 305–320.e24
- Rhodes JD, Mazza D, Nasmyth KA, Uphoff S (2017) Scc2/Nipbl hops between chromosomal cohesin rings after loading. *Elife* 6: e30000
- Riggs AD (1990) DNA methylation and late replication probably aid cell memory, and type 1 DNA reeling could aid chromosome folding and enhancer function. *Philos Trans R Soc Lond B Biol Sci* 326: 285–297
- Rowland BD, Roig MB, Nishino T, Kurze A, Uluocak P, Mishra A, Beckouët F, Underwood P, Metson J, Imre R, Mechtler K, Katis VL, Nasmyth K (2009) Building sister chromatid cohesion: SMC3 acetylation counteracts an antiestablishment activity. *Mol Cell* 33: 763–774
- Saitoh N, Goldberg IG, Wood ER, Earnshaw WC (1994) Scc1: an abundant chromosome scaffold protein is a member of a family of putative ATPases with an unusual predicted tertiary structure. *J Cell Biol* 127: 303–318
- Sanborn AL, Rao SSP, Huang S-C, Durand NC, Huntley MH, Jewett AI, Bochkov ID, Chinnappan D, Cutkosky A, Li J, Geeting KP, Gnirke A, Melnikov A, McKenna D, Stamenova EK, Lander ES, Aiden EL (2015) Chromatin extrusion explains key features of loop and domain formation in wild-type and engineered genomes. *Proc Natl Acad Sci USA* 112: E6456–E6465
- Schwarzer W, Abdennur N, Goloborodko A, Pekowska A, Fudenberg G, Loe-Mie Y, Fonseca NA, Huber W, Haering C, Mirny L, Spitz F (2017) Two independent modes of chromatin organization revealed by cohesin removal. *Nature* 551: 51–56
- Seitan VC, Banks P, Laval S, Majid NA, Dorsett D, Rana A, Smith J, Bateman A, Krpic S, Hostert A, Rollins RA, Erdjument-Bromage H, Tempst P, Benard CY, Hekimi S, Newbury SF, Strachan T (2006) Metazoan Scc4 homologs link sister chromatid cohesion to cell and axon migration guidance. *PLoS Biol* 4: 1411–1425
- Seitan VC, Faure AJ, Zhan Y, McCord RP, Lajoie BR, Ing-Simmons E, Lenhard B, Giorgetti L, Heard E, Fisher AG, Flicek P, Dekker J, Merckenschlager M (2013) Cohesin-Based chromatin interactions enable regulated gene expression within preexisting architectural compartments. *Genome Res* 23: 2066–2077
- Shintomi K, Hirano T (2009) Releasing cohesin from chromosome arms in early mitosis: opposing actions of Wapl-Pds5 and Sgo1. *Genes Dev* 23: 2224–2236
- Sofueva S, Yaffe E, Chan W-C, Georgopoulou D, Vietri Rudan M, Mira-Bontenbal H, Pollard SM, Schroth GP, Tanay A, Hadjuri S (2013) Cohesin-mediated interactions organize chromosomal domain architecture. *EMBO J* 32: 3119–3129
- Spencer SL, Cappell SD, Tsai FC, Overton KW, Wang CL, Meyer T (2013) The proliferation-quiescence decision is controlled by a bifurcation in CDK2 activity at mitotic exit. *Cell* 155: 369–383
- Splinter E, Heath H, Kooren J, Palstra RJ, Klous P, Grosveld F, Galjart N, De Laat W (2006) CTCF mediates long-range chromatin looping and local histone modification in the β -globin locus. *Genes Dev* 20: 2349–2354
- Stigler J, Camdere G, Koshland DE, Greene EC (2016) Single-molecule imaging reveals a collapsed conformational state for DNA-bound cohesin. *Cell Rep* 15: 988–998
- Sumara I, Vorlaufer E, Gieffers C, Peters BH, Peters JM (2000) Characterization of vertebrate cohesin complexes and their regulation in prophase. *J Cell Biol* 151: 749–761
- Tachibana-Konwalski K, Godwin J, Van Der Weyden L, Champion L, Kudo NR, Adams DJ, Nasmyth K (2010) Rec8-containing cohesin maintains bivalents without turnover during the growing phase of mouse oocytes. *Genes Dev* 24: 2505–2516
- Tedeschi A, Wutz G, Huet S, Jaritz M, Wuensche A, Schirghuber E, Davidson IF, Tang W, Cisneros DA, Bhaskara V, Nishiyama T, Vaziri A, Wutz A, Ellenberg J, Peters J-M (2013) Wapl is an essential regulator of chromatin structure and chromosome segregation. *Nature* 501: 564–568
- Vietri Rudan M, Barrington C, Henderson S, Ernst C, Odom DT, Tanay A, Hadjuri S (2015) Comparative Hi-C reveals that CTCF underlies evolution of chromosomal domain architecture. *Cell Rep* 10: 1297–1309
- Watrin E, Schleiffer A, Tanaka K, Eisenhaber F, Nasmyth K, Peters JM (2006) Human Scc4 is required for cohesin binding to chromatin, sister-chromatid cohesion, and mitotic progression. *Curr Biol* 16: 863–874
- Watrin E, Kaiser FJ, Wendt KS (2016) Gene regulation and chromatin organization: relevance of cohesin mutations to human disease. *Curr Opin Genet Dev* 37: 59–66
- Wendt KS, Yoshida K, Itoh T, Bando M, Koch B, Schirghuber E, Tsutsumi S, Nagae G, Ishihara K, Mishihiro T, Yahata K, Imamoto F, Aburatani H, Nakao M, Imamoto N, Maeshima K, Shirahige K, Peters J-M (2008) Cohesin mediates transcriptional insulation by CCCTC-binding factor. *Nature* 451: 796–801
- Wendt KS, Peters JM (2009) How cohesin and CTCF cooperate in regulating gene expression. *Chromosome Res* 17: 201–214
- Wingett S, Ewels P, Furlan-Magaril M, Nagano T, Schoenfelder S, Fraser P, Andrews S (2015) HiCUP: pipeline for mapping and processing Hi-C data. *F1000Research* 4: 1310
- de Wit E, Vos ESM, Holwerda SJB, Valdes-Quezada C, Versteegen MJAM, Teunissen H, Splinter E, Wijchers PJ, Krijger PHL, de Laat W (2015) CTCF binding polarity determines chromatin looping. *Mol Cell* 60: 676–684
- Yeong FM, Hombauer H, Wendt KS, Hirota T, Mudrak I, Mechtler K, Loregger T, Marchler-Bauer A, Tanaka K, Peters JM, Ogris E (2003) Identification of a subunit of a novel kleisin- β /SMC complex as a potential substrate of protein phosphatase 2A. *Curr Biol* 13: 2058–2064
- Zhang Y, Liu T, Meyer CA, Eeckhoute J, Johnson DS, Bernstein BE, Nussbaum C, Myers RM, Brown M, Li W, Liu XS (2008) Model-based analysis of ChIP-Seq (MACS). *Genome Biol* 9: R137
- Zuin J, Dixon JR, van der Reijden MIJA, Ye Z, Kolovos P, Brouwer RWW, van de Corput MPC, van de Werken HJC, Knoch TA, van Ijcken WFJ, Grosveld FG, Ren B, Wendt KS (2014) Cohesin and CTCF differentially affect chromatin architecture and gene expression in human cells. *Proc Natl Acad Sci USA* 111: 996–1001